1949

Nanoscale investigation of diffusion and solid state reactions of Ni/Si and Ag/Au thin film systems

PhD Thesis

Shenouda Shanda Shenouda Fam

Supervisor

Prof. Dr. Dezső L. Beke

Department of Solid State Physics
Faculty of Science and Technology
PhD School in Physics
University of Debrecen
Debrecen, Hungary
2015

Ezen értekezést a Debreceni Egyetem Természettudományi Doktori Tanács Fizikai Tudományok Doktori Iskolájának Szilárdtestfizika és anyagtudomány programja keretében készítettem a Debreceni Egyetem természettudományi doktori (PhD) fokozatának elnyerése céljából.

Debrecen, 2015. . . . . . .

Shenouda Shanda Shenouda Fam

I prepared this PhD thesis in the framework of the Solid State Physics and Materials Science program of the PhD School in Physics for the PhD title on Science at the University of Debrecen.

Debrecen, 2015. . . . . . .

Shenouda Shanda Shenouda Fam

Tanúsítom, hogy Shenouda Shanda Shenouda Fam *doktorjelölt 2012- 2015 között a fent megnevezett Doktori Iskola Szilárdtestfizika és anyagtudomány programjának keretében irányításommal végezte munkáját. Az értekezésben foglalt eredményekhez a jelölt önálló alkotó tevékenységével meghatározóan hozzájárult. Az értekezés elfogadását javasolom.*

Debrecen, 2015. . . . . . .

Prof. Dr. Beke Dezső

Témavezető

I certify that Shenouda Shanda Shenouda Fam *candidate for the PhD degree did his work under my supervision in the framework of the Solid State Physics and Materials Science program between 2012- 2015. The candidate achieved a determining role to the results in this thesis by his self-supporting and creative activity. I propose to accept the dissertation.*

Debrecen, 2015. . . . . . .

Prof. Dr. Dezső L. Beke

Supervisor

Nanoscale investigation of diffusion and solid state reactions of Ni/Si and Ag/Au thin film systems

Értekezés a doktori (Ph.D.) fokozat megszerzése érdekében
a **Fizika** tudományágban
Desirtation to obtain the doctoral (Ph.D.) degree in Physics

Írta: **Shenouda Shanda Shenouda Fam,** fizika MSc
Prepared by: **Shenouda Shanda Shenouda Fam,** MSc in Physics

Készült a Debreceni Egyetem **Fizikai Tudományok** Doktori Iskolája
Szilárdtestfizika és anyagtudomány programja keretében
University of Debrecen, Doctoral School of Physics
within the framework of Solid State Physics and Material Science program

Témavezető/Supervisor:**Prof. Dr. Dezső L. Beke**

A doktori szigorlati bizottság/The doctoral exam committee:

elnök/Chairman:	Dr. Ferenc Kun	……..
tagok/Members:	Dr. Gábor Erdélyi	……..
	Dr. István Groma	……..

A doktori szigorlat időpontja/The doctoral exam date: 2015 June 09

Az értekezés bírálói/The thesis reviewers:

Dr. ……..	……..
Dr. ……..	……..

A bírálóbizottság /The committee for the defense:

Chairman:	Dr. ……..	……..
Members:	Dr. ……..	……..
	Dr. ……..	……..
	Dr. ……..	……..
	Dr. ……..	……..

Az értekezés védésének időpontja/Date of the defense of the thesis: 2015. …… … .

I dedicate this Doctor of Philosophy thesis to my mother, my brother Mina and to the spirit of my father. Also, I dedicate this thesis to my future wife.

Contents

List of abbreviations and symbols

(CMOS)	Complementary metal-oxide-semiconductors
(MSD)	Metallic source/drain
(MOSFETs)	Metal-oxide-semiconductor field effect transistor
(ULS IC)	Ultra-large-scale integrated circuits
(GB)	Grain boundary
(DIGM)	Diffusion induced grain boundary motion
(DIR)	Diffusion induced recrystallization
μ_A	Chemical potential of A material
μ_{Ao}	Chemical potential of pure A material
J_A	Flux of A atoms
J_B	Flux of B atoms
L_{AA}	Onsager coefficient
k_B	Boltzmann constant
T	Absolute temperature
c_A	Atomic fraction (concentration) of A atoms

c_B	Atomic fraction (concentration) of B atoms
Ω	Atomic volume
Ω_A	Atomic volume of A atoms
Ω_B	Atomic volume of B atoms
γ_A	Activity coefficient of A atoms
ρ_A	Number of A atoms per unit volume
ρ_B	Number of B atoms per unit volume
Φ	Thermodynamic factor
D_A	Intrinsic diffusion coefficient of A material
D_B	Intrinsic diffusion coefficient of B material
n	Number of atoms or moles per unit area
n_1	Number of atoms in plane 1 per unit area
n_2	Number of atoms in plane 2 per unit area
a	Distance between neighboring atoms (the lattice distance)
Γ	Jump frequency
Γ_{12}	Jump frequency from plane 1 to 2
Γ_{21}	Jump frequency from plane 2 to 1
Γ_o	Average jump frequency
Γ_I	Jump frequency across the interface
D^A	Brownian diffusion coefficient of A material
z	Vertical coordination number

F_{ch}	Pure chemical driving force
v	Convective velocity
F_p	Pressure driving forces
p	Pressure
D	Diffusion coefficient
T_m	Melting temperature
v_K	Kirkendall-velocity
$\vec{J}'_A$	Flux of A atoms in the laboratory frame
$\vec{J}'_B$	Flux of B atoms in the laboratory frame
$\widetilde{D}$	Chemical or interdiffusion coefficient
$\widetilde{D}_D$	Darken interdiffusion coefficient
$\widetilde{D}_{NP}$	Nernst-Planck interdiffusion coefficient
λ	Boltzmann new variable
t	Time
x	Distance in x direction, position of the interface
y	Distance in y direction
M	Matano plane
Δx	Shift of the interface
v_x	Shift velocity of a plane or interface
ξ	Thickness of the growing phase
K	Growth rate constant
η	An intermediate phase

δ	Thickness of grain boundary
d_o	Grain size
D'	Grain boundary diffusion coefficient
D_{eff}	Effective diffusion coefficient
g	Grain boundary fraction
P	Parameter ($P = \delta D'$)
α'	Parameter ($\alpha' = \delta/\sqrt{Dt}$)
β'	Parameter ($\beta' = \frac{P}{2D\sqrt{Dt}}$)
$\bar{c}$	Laterally averaged (tracer) composition
J_I	Flux of A atoms across the A/AB interface
v_I	Shift velocity of the A/AB interface
α	Proportionality factor
Δc_1	Composition width of the interface
Δc_p	Composition range where the AB phase exists
Δn	Difference of the number of A atoms in two neighbouring planes per unit surface
$-(\frac{\Delta c}{a})$	Concentration gradient
Δx_c	Critical thickness at which the transition from linear to parabolic happens
H	Film thickness
c'_A	Concentration of A atoms in the GB
c'_B	Concentration of B atoms in the GB

D'_A	Grain boundary diffusion coefficient of A material
D'_B	Grain boundary diffusion coefficient of B material
q	Parameter ($q = q_A c'_A + q_B c'_B$)
q_A	Proportionality factor between the GB composition and the composition deposited by the moving boundary
D'^D	Darken like interdiffusion coefficient in the GB
D'^{NP}	Nernst-Planck like interdiffusion coefficient in the GB
s	Coefficient of segregation
ζ	Height of GB step
b_n	Burgers vector
(GBDIREAC)	Grain boundary diffusion-induced reaction layer formation
(RTA)	Rapid thermal annealing
(SNMS)	Secondary neutral mass spectrometry
(TEM)	Transmission electron microscopy
a-Si	Amorphous-Si
c-Si	Crystalline-Si
(DCS)	Differential scanning calorimetry
(XRD)	X-ray diffraction
(DC)	Direct current
β (FWHM)	Full width at half maximum
λ'	Wavelength
θ	Angle of diffraction

L	Average migration distance
c_e	Equilibrium composition of the growing phase
c	Average concentration
Q_g	Activation energy
K_g	Growth constant
Q_f	Activation energy obtained from the temperature dependence of linear growth constant
K_f	Linear growth constant
ρ^*	Volume fraction
R	Resistance
k	Conductivity
V	Volume
t'	Corrected time after subtracting the time required to fill the boundary t_o
X	Shift of the A/AB interface
Y	Shift of the AB/B interface
c_{sat}	Saturation value of concentration

Motivation

Nowadays, the increased demand for minimizing the size of any kind of device became technologically a chief challenge. This field of science plays a vital role in the present technologies. The down scale can affect significantly the properties of the product and improve their performance. Thus, the nanoscale investigation of diffusion and solid state reactions in thin film systems is very important for many technologies and applications such as complementary metal-oxide-semiconductors (CMOS), metallic source/drain (MSD) MOSFETs and in the ultra-large-scale integrated circuits (ULS IC). These investigations contribute to better understanding of the details of the reactions.

Silicides are very important contact materials in such applications. Nickel mono-silicide (NiSi) has advantages over the other silicides especially due to its lower resistivity and the good contact to other materials. We report a process to obtain homogenous NiSi layers by grain boundary diffusion induced solid state reaction between nanocrystalline-Ni_2Si thin film and crystalline(c)-Si at low temperatures (180-200^oC). We could show the existence of certain temperature-time and thickness-time windows in side of which the formation of NiSi takes place, allowing the production of the requested NiSi layer in a well-controlled way down to about 5 nm thickness.

Then, we studied the low temperature (180^oC) solid state reactions in Ni/c-Si and Ni/amorphous(a)-Si by following the kinetics of the growth of the product layer and the shift of individual interfaces as well. Also, the effect of Pt in both systems was investigated. In usual investigations, the

thickness of the reaction layer is determined as function of the annealing time. However, the growth of a reaction layer is always a result of the *simultaneous shift of two interfaces* bordering the given phase. Thus, for a deeper understanding of such nanoscale solid state reactions, following the kinetics of both individual interfaces and thus the experimental methods of their determination are very important. Knowing these one can easily compose their combination for the interpretation of the growth kinetics of phases and the controllable formation of ultrathin metal silicide films. Thus, Ni/Si system can be used as a model system for better understanding the details of the early stages of the solid state reactions at nanoscale. This model can be applied in other systems.

During the interdifussion in binary system at low temperatures where the bulk diffusion is completely frozen, the inequality of the grain boundary (GB) fluxes can lead to diffusion induced grain boundary motion (DIGM) and also to porosity formation along the GBs. Since there are only few results on porosity formation at the GBs (and all the studies were done on the microscale, and at relatively high temperatures), we were interested in investigating the nanoporosity at low temperatures. In addition in most of the previous studies the DIGM was studied in the slower component of the diffusion couple. Thus we investigated simultaneously the DIGM on both sides. We could provide clear experimental evidence on the porosity formation along GBs and triple junctions in Ag during intermixing in Ag/Au thin film system at low temperature (120-200^{o}C). The understanding of this process is important for basic understanding of many technological aspects of nanomaterials.

Chapter 1

Introduction

In order to understand and control the solid state reactions in the matter on the nanoscale, we need to understand the phenomena of diffusion. The diffusion is atomic scale mixing in the matter whatever it has an ordered or disordered structure [1,2]. There are a lot of diffusion mechanisms e.g. direct and indirect interstitial mechanisms, ring mechanism, vacancy mechanism ...etc [2]. In this chapter expressions describing the atomic flux, which is the number of atoms crossing a unit area per unit time, are explained. The two equations of Fick are also presented. Then, diffusion in both bulk and grain boundaries will be described. Furthermore, the nucleation and growth of layers, diffusional kinetics and the solid state reactions in thin films at low temperature are summarized.

1.1. Atomic fluxes and Fick law

In a binary AB system the flux of atoms A - if there is no driving forces other than given by the gradients of the chemical potential, μ_A, - can be expressed as [2-4]:

$$J_A = -L_{AA}\, grad\, \mu_A \,, \tag{1.1}$$

where L_{AA} is the Onsager coefficient and μ_A is given by [5]:

$$\mu_A = \mu_{Ao} + k_B T \ln \gamma_A c_A \,, \tag{1.2}$$

where μ_{Ao} is the chemical potential of pure A material, k_B is the Boltzmann constant and T is the temperature. c_A and γ_A are the atomic fraction and the activity coefficient, respectively. Combining Eqs. (1.1) and (1.2) and using that $\rho_A\, \partial c_A/\partial \rho_A = c_A$ and $\rho_A + \rho_B = constant$, where ρ_A is the number of A atoms per unit volume ($c_A/\Omega=\rho_A$ where Ω is the atomic volume), the following relation is obtained [4]:

$$J_A = -\frac{k_B T L_{AA}}{\rho_A}\left[1+\frac{\partial \ln \gamma_A}{\partial \ln c_A}\right] grad\ \rho_A = -\frac{k_B T L_{AA}}{\rho_A}\ \Phi grad\ \rho_A$$

$$= -D_A grad\ \rho_A, \qquad (1.3a)$$

where Φ is the thermodynamic factor and D_A is the intrinsic diffusion coefficient.

It is clear that Eq. (1.3a) is just the well-known Fick's first law. In general the diffusion flux and concentration are functions of time and position. In one dimension, Eq. (1.3a) can be written as:

$$J_A = -\frac{k_B T L_{AA}}{\rho_A}\left[1+\frac{\partial \ln \gamma_A}{\partial \ln c_A}\right].\frac{d\rho_A}{dx} = -D_A \frac{d\rho_A}{dx}\,. \qquad (1.3b)$$

According to Fig. 1.1, if the number of atoms or moles per unit area, n, varies slightly with the distance perpendicular to the atomic planes, we can write:

$$n_1 = n - \frac{dn}{dx}\,\frac{a}{2} \quad \text{and} \quad n_2 = n + \frac{dn}{dx}\,\frac{a}{2}\,, \qquad (1.4)$$

and the flux of atoms A can be also expressed as [4]:

$$J_A = n_1\Gamma_{12} - n_2\Gamma_{21}, \qquad (1.5a)$$

where Γ_{12} and Γ_{21} are the jump frequencies from plane 1 to 2 and in the opposite direction, respectively. Combing these equations and using $\frac{n}{a} = \rho$, we obtain:

$$J_A = -a^2\Gamma_o \frac{d\rho}{dx} + \rho a(\Gamma_{12} - \Gamma_{21}), \text{ with } \frac{\Gamma_{12}+\Gamma_{21}}{2} = \Gamma_o\,. \qquad (1.5b)$$

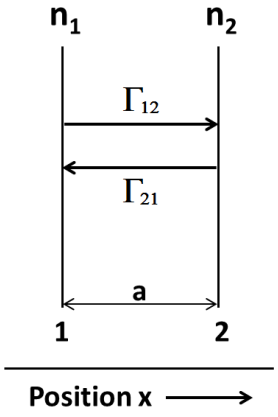

Fig. 1.1. Jump frequencies between neighboring atomic planes.

The first term in both Eqs. (1.3b) and (1.5b) corresponds to the Brownian-migration (random walk) of atoms [2,6]. In this case, $\Gamma_{12} = \Gamma_{21}$ and a current, perpendicular to the planes, arises only due to the difference between the numbers of atoms in the two planes. The Brownian diffusion coefficient, D^A, corresponding to this term can be expressed as:

$$D^A = \frac{k_B T L_{AA}}{\rho_A} = a^2 \Gamma_o \,, \tag{1.6}$$

Sometimes the average jump frequency, Γ_o, is expressed as the product of the vertical coordination number z and jump frequency Γ. Note that in case of vacancy mechanism Γ_o contains the product of vacancy concentration and vacancy-atom exchange frequency.

The second term in Eqs. (1.3b) and (1.5b) corresponds to the presence of any driving force resulting in different jump frequencies between the two atomic planes ($\Gamma_{12} \neq \Gamma_{21}$). For example, if $\gamma_A = 1$ (dilute or ideal solid solution), this so called chemical term is zero. The effect of the pure chemical driving force, $F_{ch} = -k_B T \; grad \, (\ln \gamma_A)$, can be expressed as a convective term so Eqs.(1.3a), (1.3b) and (1.5b) can be given in the following form [4]:

$$J_A = -D^A . grad \, \rho_A + \rho_A v \;, \tag{1.7}$$

where the convective velocity is given by [4]:

$$v = a(\Gamma_{12} - \Gamma_{21}) = -D^A \, grad \, (\ln \gamma_A) = \frac{D^A}{k_B T} F_{ch} \, . \tag{1.8}$$

Eq. (1.8) is the well-known Nernst-Einstein equation. The effect of other driving forces (e.g. temperature gradient, electric potential gradient, pressure gradient, etc.) can be treated similarly [2,7] and e.g. in the presence of a pressure gradient $F_p = -\Omega \, grad \, p$.

1.2. Equations for diffusion

Any real crystal has lattice defects such as dislocations, grain boundaries and free surfaces. Because diffusion along such defects is usually higher than in the bulk, they are denoted as diffusion short-circuits of high diffusivity (see Fig. 1.2) [4].

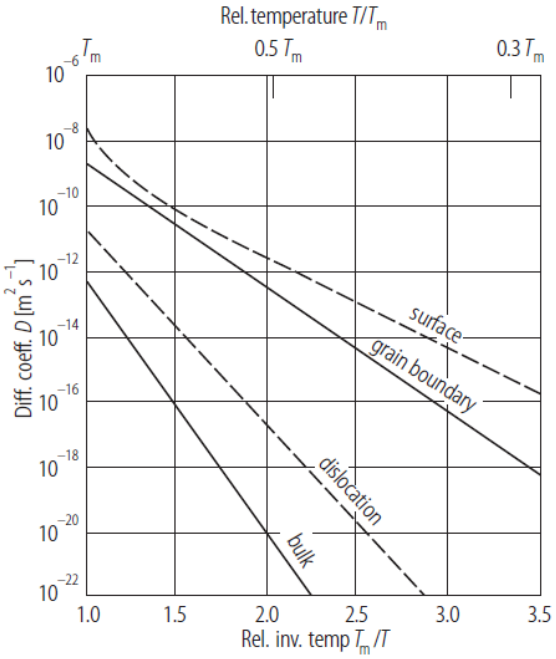

Fig. 1.2. Schematic illustration of different diffusion coefficients D on the inverse temperature relative to the melting temperature T_m/T (Arrhenius diagram).

1.2.1. Bulk diffusion

For non-steady diffusion problems, the continuity equation should be taken into account. It has the following form for particles undergoing no reactions;

$$\frac{\partial \rho_A}{\partial t} + \text{div}\, J_A = 0. \tag{1.9}$$

Combining Eq. (1.3a) with Eq. (1.9), we can obtain the Fick second law:

$$\frac{\partial \rho_A}{\partial t} = \text{div}\,(D_A\, grad\, \rho_A). \tag{1.10}$$

When the concentration varies only along the x direction (in isotropic solids), Eq. (1.10) becomes:

$$\frac{\partial \rho_A}{\partial t} = \frac{\partial}{\partial x}\left(D_A\, \frac{\partial \rho_A}{\partial x}\right). \tag{1.11}$$

For constant diffusion coefficients, Fick's second law will be: ($\frac{\partial \rho_A}{\partial t} = D_A \frac{\partial^2 \rho_A}{\partial x^2}$), which can be simply solved.

1.2.1.1. Chemical or interdiffusion

If two different materials are in contact, the diffusional mixing can be described by Eq. (1.9). Since the atomic currents between the partners A and B of the diffusion couple are usually not equal (as shown in Fig. 1.3), there will be a resultant volume transport ($J_A\Omega_A \neq J_B\Omega_B$). Also, in the case of vacancy mechanism, there is a resultant vacancy flow proportional to the difference of J_A and J_B. This is equivalent to the creation of a non-uniform stress-free strain: contractions arise on one side of the diffusion zone, while extensions will arise on the other side. The resulting stress field contributes to the atomic currents across the driving force $F_p = -\Omega\, grad\, p$ [4,8].

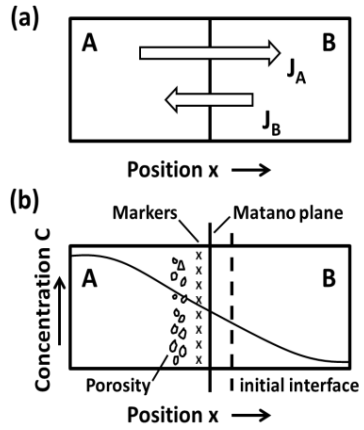

Fig. 1.3. (a) Atomic currents J_A and J_B, (b) the result of interdiffusion schematically in an AB diffusion couple.

If the relaxation of stresses is fast and almost complete, the additional term to Eqs. (1.3a) and (1.3b), caused by the stress gradient as a driving force, can be neglected.

The relaxation of stresses is equivalent to a convective transport in the diffusion zone. For vacancy mechanism, expansions and contractions on both sides of the diffusion zone can be realized by annihilation and creation of vacancies at edge dislocations. This will lead to an additional convective term – in the laboratory frame – to the right hand side of Eq. (1.7): $\rho_A v_K$, where v_K is the Kirkendall-velocity [4]. This limit was treated by Darken [9] and its results were widely used in the evaluation of chemical or interdiffusion experiments. If the number of lattice sites is conserved [10], $\frac{\partial(\rho_A+\rho_B)}{\partial t} = 0$, we will obtain [4]:

$$\vec{j}'_A = -\widetilde{D}\ grad\ \rho_A = \vec{j}'_B = \widetilde{D}\ grad\ \rho_B\ . \qquad (1.12)$$

The prime indicates that the currents now are expressed in the laboratory frame. It is clear that the diffusion mixing can be described by a unique diffusion coefficient for both components called chemical or interdiffusion coefficient $\widetilde{D}$;

$$\widetilde{D}_D = c_B D_A + c_A D_B = \rho_B \Omega_B D_A + \rho_A \Omega_A D_B \ . \tag{1.13}$$

Furthermore, the Kirkendall-velocity can be expressed as [4]:

$$v_k = (D_A - D_B) grad\ c_A \ . \tag{1.14}$$

The shift of lattice planes with respect to axes fixed at the end of the sample can be determined by inserting inert markers (e.g. insoluble particles, wires) into the initial interface and by measuring their shift [4].

When the above relaxation processes are restricted, we will be in the second limit (Nernst-Plank limit). In this case, there is no stress relaxation at all (and thus $v_k \cong 0$). Now an additional term, proportional to the stress gradient should be added to the right hand side of Eqs. (1.3a) and (1.3b) and in this case the mixing process is controlled by [10,11]:

$$\widetilde{D}_{NP} = \frac{D_A \,.\, D_B}{c_A D_A + c_B D_B} \ . \tag{1.15}$$

After an initial transient period, the developed pressure gradient makes the two currents equal. This means that the transport will be determined by the slower intrinsic diffusion coefficient (series coupling of currents) in contrast to the Darken's limit (parallel coupling) where the chemical diffusion coefficient is determined by the faster one [4].

The resultant vacancy flow can lead to a super-saturation and precipitation of vacancies, i.e. porosity formation, in the diffusion zone. It was observed that there is a competition between such porosity formation and the Kirkendall-shift. The application of small hydrostatic pressures (~100 bar) can prohibit the porosity formation [12,13], due to blocking the increase of the sample volume by the external pressure. At the same time, this enhances the vacancy sink efficiency of dislocations in the diffusion zone [4].

Boltzmann transformation

By introducing a new variable $\lambda = x/\sqrt{t}$, Eq. (1.11) will be transformed to an ordinary differential equation [4]:

$$-\frac{\lambda}{2}\frac{d\rho}{d\lambda} = \frac{d}{d\lambda}\left(\widetilde{D}\frac{d\rho}{d\lambda}\right) \tag{1.16}$$

The solution of Eq. (1.16) is a $\rho(\lambda)$ function. This transformation can be applied if the initial and boundary conditions can be expressed as functions of λ only. This will be the case in a diffusion couple consisting of slabs thick enough as compared to $2\sqrt{Dt}$. $\widetilde{D}$ can be evaluated from the Boltzmann-Matano equation [4]:

$$\widetilde{D} = -\frac{1}{2}\frac{\int_{\rho_1}^{\rho}\lambda\, d\rho}{\left(\frac{d\rho}{d\lambda}\right)_{\rho}} = -\frac{1}{2t}\frac{\int_{\rho_1}^{\rho} x\, d\rho}{\left(\frac{d\rho}{dx}\right)_{\rho}}. \tag{1.17}$$

The origin of x, denoted as the Matano plane M, is determined by the following condition [4]:

$$\int_{\rho_1}^{\rho_2}\lambda\, d\rho = 0 = \int_{\rho_1}^{\rho_2} x\, d\rho = 0. \tag{1.18}$$

This interface fixes two equal areas on the $\rho(x)$ or $c(x)$ profile (as shown in Fig. 1.4); through this plane equal amounts of the material moved in the positive and negative directions. For concentration independent $\widetilde{D}$, the Matano plane coincides with the initial position of the interface [4].

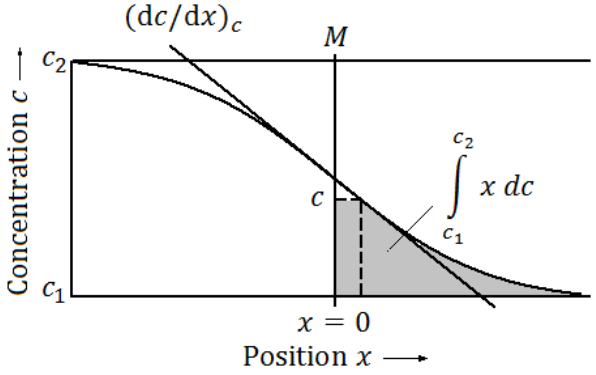

Fig. 1.4. Illustration of the calculation of the chemical or interdiffusion coefficient from the concentration profile according to the Boltzmann-Matano method.

Because the solution of Eq. (1.16) is a function of $\lambda = x/\sqrt{t}$ only, a plane of constant concentration shifts as the square root of time; $x \sim\sqrt{t}$. This

is also valid for the Kirkendall-shift. Similarly, in multiphase diffusion (i.e. when there is no complete solid state miscibility of the components and there exist intermetallic compound as shown in Fig. 1.5) the Boltzmann-Matano method is also applicable, because the phase boundaries are points of constant concentration. It is clear that the thickness ξ of the growing phase should also follow the parabolic law (if the role of the reactions at the interfaces and the possible competition between simultaneously growing phases is neglected [2, 4]);

$$\xi^2 = Kt, \tag{1.19}$$

where K is the *growth rate constant* and can be related to the intrinsic diffusion coefficients and to the thermodynamic data [4].

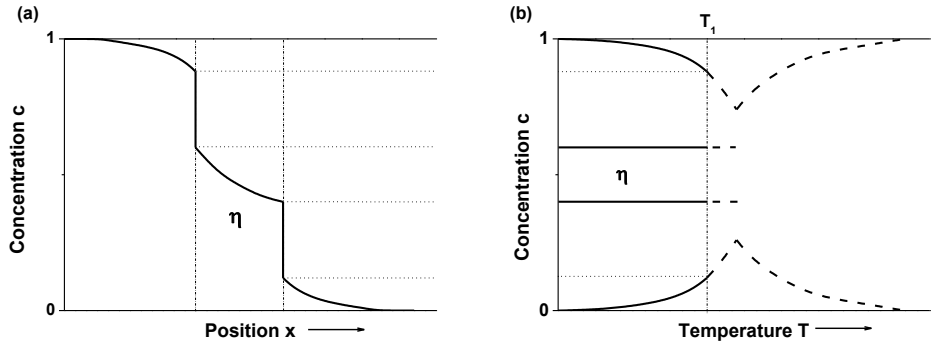

Fig. 1.5. Concentration distribution in the diffusion zone, when the constituents have restricted solubility (**a**) and an intermediate phase η exists also in the phase diagram (**b**).

It is interesting that in the case of diffusion on the nanoscale [14] there exist a paradox: from Eq. (1.19) $\xi \sim \sqrt{t}$ i. e. the shift velocity of a plane with constant composition (e.g. an interface) tends to infinite as the time tends to zero:

$$v_x = \frac{dx}{dt} \propto \frac{1}{2\sqrt{t}} \Rightarrow \lim_{t\to 0} v_x = \infty. \tag{1.20}$$

This means that the growth rate of the diffusion zone will be infinite when t goes to zero. It can be shown from atomistic simulations [15] that this paradox can be resolved if one takes into account that even if at the beginning, when the compositions on the two neighboring atomic planes are 1 and 0, i.e. the gradient ($\cong -1/a$) is very large, the jumps across the interface should be restricted by the finite atomic jump across the interface (finite interface permeability): see also below. Note that in this case, since $v_x \sim J \equiv const.$, where now J is the flux across the interface, $x \sim t$, i.e. the interface shifts linearly with time. Thus below certain diffusion distance (time) the shift is linear and above it proportional to the square root of time: this is called linear-parabolic law [15].

1.2.2. Grain boundary diffusion

In general the grain boundary, GB, is an internal surface between two adjacent grains. It can be a curved surface, but here only planar boundaries are considered. The thickness of these boundaries, δ, is estimated about few atomic layers (δ=0.5nm is a good estimate). The constrain of the two differently oriented grains, being in contact, is strong enough to make the GB structure different from amorphous. This allows the formation of periodic GB structure in special cases.

In mathematical models describing the GB diffusion, the boundary is supposed to be a homogeneous slab of thickness δ (as shown in Fig. 1.6), with a high diffusivity, D', as compared to the bulk (D_1, D_2).

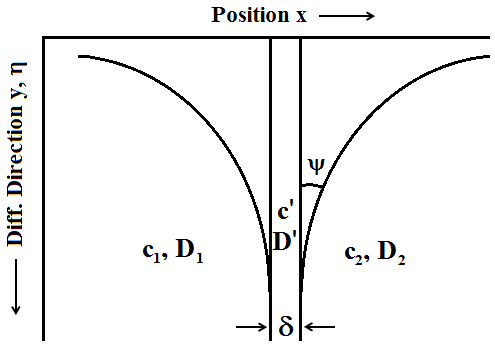

Fig. 1.6. Isoconcentration contour according to Fisher's model for grain boundary diffusion.

As proposed by Harrison [16], depending on the time of the heat treatment and on the grain size, d_o, three types of kinetic behavior can be distinguished (as shown in Fig. 1.7).

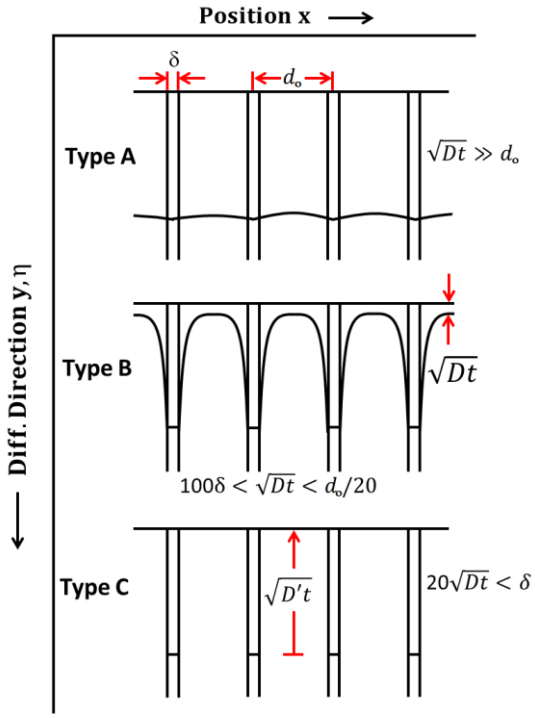

Fig. 1.7. Different types of diffusion regimes for grain boundary diffusion.

- **Type-A kinetics**

Here the diffusion fields, developed around each boundary in the bulk, overlap since $\sqrt{Dt} \gg d_o$. This can be for large enough annealing time or for small enough grain size [1]. Thus, the diffusion process can be characterized by an effective diffusivity [4]:

$$D_{eff} = gD' + (1-g)D, \qquad (1.21)$$

where g is the grain boundary fraction.

This Hart's equation is obtained simply by averaging over the whole period of the migration of the diffusant; the time fractions spent in the

boundary and inside the grains are proportional to g and $1-g$, respectively [4,17].

- **Type-B kinetics**

In this type the volume diffusion length is shorter than the GB diffusion length. So there is no uniform diffusion front line, but there is diffusion into the grains [1]. This is the generally realized situation in most experiments. It can be shown [4] that if

$$\alpha' = \delta/\sqrt{Dt} < 0.01 \quad \text{and} \quad \beta' = \frac{P}{2D\sqrt{Dt}} > 10, \tag{1.22}$$

(where $P = \delta D'$ and D_1=D_2=D), from the solution of diffusion equation both for thin film or constant source initial and boundary conditions, that the parameter P can be expressed as [4]:

$$P = \left(-\frac{\partial ln\, \bar{c}}{\partial y^{6/5}}\right)^{-5/3} \left(\frac{4D}{t}\right)^{1/2} A^{5/3}, \tag{1.23}$$

where y is the direction of diffusion and $A \cong 0.78$ [18].

It is an advantage that the form of the tracer penetration function, $\ln \bar{c}$ vs. $y^{6/5}$, (where $\bar{c}$ is the laterally averaged (tracer) composition in the plane perpendicular to y) is practically independent of the boundary conditions, and the product $P = \delta D'$ can be determined, if the bulk diffusion coefficient is known [4]. Note that for impurity diffusion the parameter P contains the GB segregation factor, s, too: $P = \delta D' s$.

- **Type C kinetics**

This type refers to the limit when the bulk diffusion length $\sqrt{Dt}$ is negligible as compared to δ. In this case the diffusion is restricted to the grain boundaries only and direct determination of D' is possible [4].

1.3. Solid state reactions

1.3.1. Nucleation and growth of layers and diffusional kinetics

The above mentioned problem of linear-parabolic growth of reaction products in solid state reactions is as old as the experimental investigation of

this phenomenon. Solid state reactive diffusion in general is a rather complex process because it involves both diffusion and phase transformation.

Consider a binary diffusion pair (A/B). For simplicity, we restrict ourselves to one dimension and assume formation of one AB intermetallic compound. Also, only one of the components, A, is assumed mobile. Then first AB nuclei will form at the original interface and grow continuously until they will meet each other and form a continuous layer with A/AB and AB/B interfaces parallel with the original interface (see Fig. 1.8).

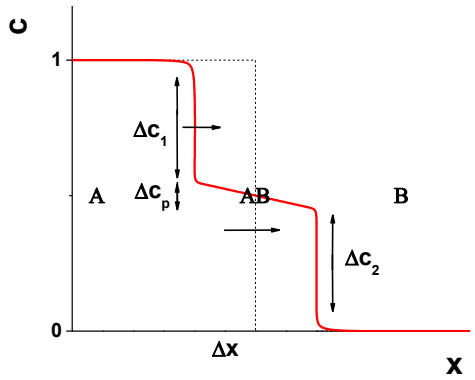

Fig. 1.8. Composition profile versus distance schematically for growth of AB intermetallic layer.

The position of the A/AB interface and its shift are denoted by x and Δx, respectively. The flux of A atoms across this interface, J_I, is given by:

$$J_I = \frac{\alpha v_I}{\Omega} = \frac{\alpha}{\Omega}\frac{d(\Delta x)}{dt}, \tag{1.24}$$

where v_I is the shift velocity. This is the consequence of the conservation of matter (Stephan's law) and the $\alpha \leq 1$ proportionality factor can be estimated from the composition width of the interface, Δc_1. On the other hand, the diffusion flux of A inside the AB phase can be given as, if $grad\, c = -\Delta c/\Delta x$:

$$J = -\frac{D}{\Omega}\, grad\, c = \frac{D}{\Omega}\frac{\Delta c_p}{\Delta x}, \tag{1.25}$$

where Δc_p is the composition range where the AB phase exists, and $D = za^2\Gamma$.

Expressions (1.24) and (1.25) should be equal to each other (there is no either deposit of A atoms or take up of extra A atoms), i.e.

$$\frac{d(\Delta x)}{dt} = \frac{D}{\alpha}\frac{\Delta c_p}{\Delta x}\,. \tag{1.26}$$

The integral of this leads to:

$$\Delta x \sim \sqrt{t}, \tag{1.27}$$

This is the well-known parabolic diffusion kinetics ($(\Delta x)^2 \sim t$) of phase growth.

The above description – similarly as the macroscopic Fick I law – is valid for continuous materials. It is not valid for very short distances and large composition gradients. This is due to the discrete character of the crystal: for the initial contact of pure A and B the composition gradient would be infinite in the above continuum limit, while in discrete lattice it will be $-1/a$, where a is the lattice spacing. Thus the flux is infinite in continuum approach and finite in more realistic atomic approximation. This also means that at atomic scale the flux of atoms across the interface is finite and can be expressed as [15]:

$$J_I = z\Gamma_I(n_1 - n_2) \tag{1.28}$$

where n_1 and n_2 are the number of A atoms in the planes 1 and 2, respectively, per unit surface. Using the relation between surface and bulk density ($n = \rho a = \frac{c}{\Omega}a$):

$$(n_1 - n_2) = \frac{c_1 - c_2}{\Omega}a = \frac{a^2}{\Omega}\frac{c_1 - c_2}{a} = -\frac{a^2}{\Omega}\frac{\Delta c}{\mathrm{a}} \tag{1.29}$$

where ($n_1 > n_2$) and ($-\frac{\Delta c}{\mathrm{a}}$) is the concentration gradient: for contact of pure A and B, $\Delta c \cong -1 \cong constant$ can be taken at the beginning. Thus,

$$J_I = z\Gamma_I \frac{a^2}{\Omega} \frac{1}{a} \tag{1.30}$$

Now, Eqs. (1.24) and (1.30) should be equal to each other at least for Δx values for which (1.30) will be still less than the classical flux given by (1.25). In this comparison it is important to realize that in D present in (1.25) the jump frequency Γ is the atomic jump frequency in the AB compound and it is different from Γ_I:

$$\frac{d(\Delta x)}{dt} = \frac{za\Gamma_I}{\alpha}. \tag{1.31}$$

Since the right hand side is approximately constant, the integral of this gives

$$\Delta x \sim t \tag{1.32}$$

This is the linear growth law. For short annealing times, i.e. for small values of Δx the composition gradient in (1.25) would be so large that it would be larger than (1.30) and in this case the interface shift will be determined by the small flux (1.30). This is why this linear shift is called interface transfer controlled mechanism and the right hand side of (1.31) is the so-called interface transfer coefficient (having a dimension m/s). Of course with increasing time (or with increasing Δx) the flux given by (1.25) will be less than the (constant) flux (1.30) and there will be a transition to parabolic regime. From the equality of (1.26) and (1.31) the critical thickness at which the above transition happens is expressed as:

$$\Delta x_c = \Delta c_p \frac{D}{za\Gamma_I} = \Delta c_p \frac{a\Gamma}{\Gamma_I} \tag{1.33}$$

Since (Δc_p) is in the order of 0.1, the value of Δx_c depends on the $\frac{\Gamma}{\Gamma_I}$ ratio. If it is unity, which corresponds to composition independent jump frequency; the jump frequency is the same at the interface and in the AB phase, Δx_c will be in the order of $0.1a$, i.e. the effect is not observable even on nanoscale. In the other hand, when the jump frequency has a very strong composition dependence, the $\frac{\Gamma}{\Gamma_I}$ can be 10^4 (this can be the case for many systems at low temperatures) and in this case Δx_c can be in the order of 10^4a, i.e. it can be even about 300 nm.

1.3.2. Solid state reactions in thin film systems at low temperatures

The problem of solid-state reactions between nanostructured thin films is still a challenging subject. In case of nanocrystalline films, the mass transport along different GBs can affect significantly the entire intermixing process [19]. It is well known that the GB diffusion coefficient can be rather different in GBs or triple junctions [20,21] with different structures. This process can be also characterized by a bimodal GB network with fast and slow diffusivities [19].

At low temperatures, during interdiffusion in binary systems where intermetallic layers can grow, the morphology of the formation and growth of the reaction product can be different from the usual picture observed at high temperatures, where the new continuous phases form at the initial interface growing parallel to the contact surface. It is well known that at low temperatures, where bulk diffusion processes are practically frozen, intermixing of components in binary nanocrystalline couple can happen by grain boundary migrations through the volume. Diffusion-induced grain boundary motion (DIGM) and diffusion-induced recrystallization (DIR) are the examples of such type of GB motions [23,22-24].

During DIR, a large number of new small grains are formed with different composition from the surrounding original grains due to recrystallization combined with diffusion of solute atoms along the GBs [25,26]. The nucleation of the DIR grains is suggested to be based on emission of dislocations by moving boundaries into low angle boundaries which become high angle boundaries surrounding DIR grains [26].

The other mechanism, DIGM, is a process where the presence of a solute able to diffuse along GBs causes migration of the interface leaving behind an alloyed region with different composition [25,26] (as shown in Fig. 1.9). Unbalanced fluxes of solute and solvent result in a net vacancy flux which allow climb of GB dislocations and consequent migration of the boundary.

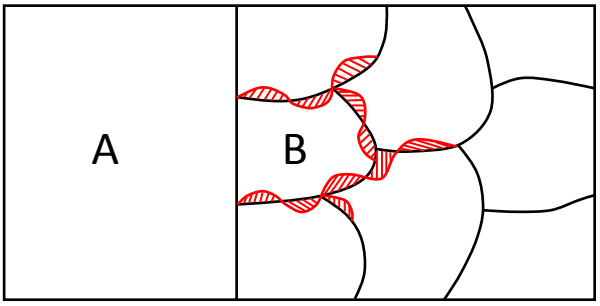

Fig. 1.9. Schematic diagram for DIGM, the red zones represent the alloyed regions left behind the moving boundaries.

Although there are still discussions in the literature about the role of chemical driving forces [27], it is more and more widely accepted that at low temperatures in both processes the driving forces are related to stress accumulation and relaxation around the moving boundary [22,28,29].

It is difficult to distinguish between DIR and DIGM experimentally [30]. DIR has mainly been investigated in binary systems with wide mutual solubility range above either the miscibility gap or the critical temperature of ordering (e.g. in Cu/Pd [30], Au/Cu [31], Ag/Pd [32], Ni/Cu [27,33]). A model interpreting DIR was even developed for such systems in [22].

The essential features of DIGM were first described by Hillert and Purdy [34] by heat-treating of polycrystalline Fe in Zn vapor at a temperature where the volume diffusion coefficient of either zinc or iron in iron is small. It was observed that the grain boundaries close to the exposed surface migrated [35].

Regarding the theoretical description, for the sake of simplicity, we can consider a free standing B film of H thickness during diffusion of A atoms from the vapor sources on both sides (Fig. 1.10)

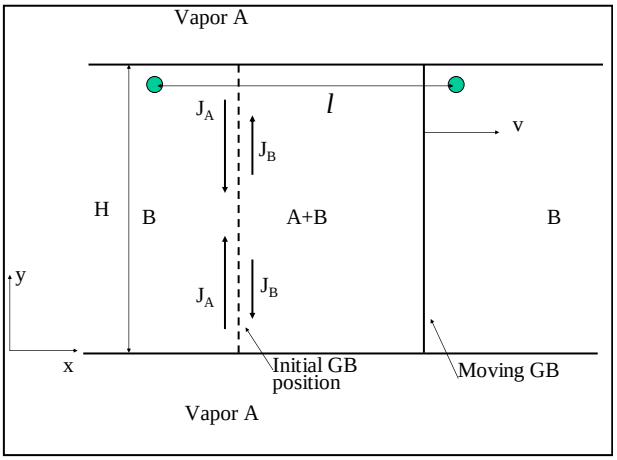

Fig. 1.10. Scheme of the GB interdiffusion process: material A diffuses into the GB of pure B from the gas phase [36].

The GB fluxes of the two species, J_A and J_B (in units of atoms per unit time and unit length: the line along which this unit length is taken is perpendicular to the plane shown in Fig. 1.10), are given by the following expressions at the beginning:

$$J_A = -\frac{1}{\Omega_A} D'_A \delta \frac{\partial c'_A}{\partial y}, \qquad J_B = -\frac{1}{\Omega_B} D'_B \delta \frac{\partial c'_B}{\partial y}, \tag{1.34}$$

where $\Omega_A = \Omega_B = \Omega$ is the atomic volume.

Since $D'_A > D'_B$, and $J_A > J_B$, accumulation of atoms (more A atom arrives in B than leaves the GB) takes place and a stress field develops normal to the boundary [37-39]. Accordingly, Eqs. (1.34) should be corrected as (see also [38]):

$$J_A = -\frac{1}{\Omega} D'_A \delta \frac{\partial c'_A}{\partial y} - \frac{D'_A c'_A \delta \, \partial\sigma/\partial y}{kT},$$

$$J_B = -\frac{1}{\Omega} D'_B \delta \frac{\partial c'_B}{\partial y} - \frac{D'_B c'_B \delta \, \partial\sigma/\partial y}{kT}. \tag{1.35}$$

Furthermore, assuming that the stresses can relax, at least partly, by the motion of the boundary along the direction x, the condition of mass conservation for both components can be written in the form;

$$\frac{\partial c'_A}{\partial t} = -\frac{\Omega}{\delta}\frac{\partial J_A}{\partial y} - \frac{v_x}{\delta}\, q_A c'_A, \qquad \frac{\partial c'_B}{\partial t} = -\frac{\Omega}{\delta}\frac{\partial J_B}{\partial y} - \frac{v_x}{\delta}\, q_B c'_B. \tag{1.36}$$

and the $q_A = f(c_A)$ factor in these expressions takes into account the transitions of extra A atoms from the GB to the bulk, as well as the transition of B atom from the bulk to the GB [36], due to the shift of the boundary with v_x velocity. The compositions of atoms in the boundary and in the bulk (c' and c, respectively) are obviously interrelated.

Now we can consider the following limits after a certain transient period. The GB fluxes are equalized either [36]:

a) by the relaxation of stresses (if this relaxation is continuous, fast and efficient enough) via the shift of the boundary and one can neglect the second terms in (1.35): Darken-type limit, or

b) by the corrections due to the stress gradients (see the second terms in (1.35)) and the GB does not move, i.e. $v_x = 0$: Nernst-Planck-type limit.

Let us see the first case a) – Neglecting the terms containing the stress gradients in (1.35) and taking the sum of the expressions given by (1.36), we get (assuming also for the sake of simplicity that D'_A and D'_B are constant and using that $c'_A + c'_B = 1$):

$$\frac{\partial c'_A}{\partial t} + \frac{\partial c'_B}{\partial t} = (D'_A - D'_B)\frac{\partial^2 c'_A}{\partial y^2} - \frac{v_x}{\delta} q\,, \tag{1.37}$$

with $q = q_A c'_A + q_B c'_B$. Since $\frac{\partial c'_A}{\partial t} + \frac{\partial c'_B}{\partial t} = 0$, Eq.(1.37) gives

$$v_x = \frac{\delta}{q}(D'_A - D'_B)\frac{\partial^2 c'_A}{\partial y^2}. \tag{1.38}$$

Putting back expression (1.38) e.g. into the first one of (1.36), one arrives at

$$\frac{\partial c'_A}{\partial t} = D'^D \frac{\partial^2 c'_A}{\partial y^2}, \tag{1.39}$$

with [36]

$$D'^D = D'_A(1 - C_A) + D'_B C_A, \tag{1.40}$$

and $C_A = \frac{q_A}{q} c'_A$.

Interestingly expression (1.40) has similar form as the bulk interdiffusion coefficient in the Darken limit but here the GB diffusion coefficient is weighted by the factor $(\frac{q_A}{q})$.

For the other limit b) – Now the stress gradient corrections compensate the differences of fluxes, and again from the condition $\frac{\partial c'_A}{\partial t} + \frac{\partial c'_B}{\partial t} = 0$ and assuming that $v_x = 0$ in (1.36), one arrives at

$$\frac{\partial (J_A + J_B)}{\partial y} = 0 \,. \tag{1.41}$$

From this condition, the

$$(\mathrm{D}'_A - D'_B)\frac{\partial^2 c'_A}{\partial y^2} + \frac{(D'_A c'_A + D'_B c'_B)\Omega}{kT}\frac{\partial^2 \sigma}{\partial y^2} + \frac{(D'_A - D'_B)\Omega}{kT}\frac{\partial \sigma}{\partial y}\frac{\partial c'_A}{\partial y} = 0 \,,$$

relation can be obtained, i.e.

$$\frac{\Omega}{kT}\frac{\partial^2 \sigma}{\partial y^2} = \frac{D'_B - D'_A}{D'_A c'_A + D'_B c'_B}\left[\frac{\partial^2 c'_A}{\partial y^2} + \frac{\Omega}{kT}\frac{\partial \sigma}{\partial y}\frac{\partial c'_A}{\partial y}\right]. \tag{1.42}$$

Putting this e.g. into the first equation of (1.35), we obtain [36]

$$\frac{\partial c'_A}{\partial t} = D'^{NP}\frac{\partial^2 c'_A}{\partial y^2}\left[1 + \frac{\frac{\Omega}{kT}\frac{\partial \sigma}{\partial y}\frac{\partial c'_A}{\partial y}}{\frac{\partial^2 c'_A}{\partial y^2}}\right], \tag{1.43}$$

with

$$D'^{NP} = \frac{D'_A D'_B}{(c'_A D'_A + c'_B D'_B)}, \tag{1.44}$$

where D'^{NP} has the form of a Nernst-Planck like interdiffusion coefficient. If the second term in the bracket can be neglected, this is the GB interdiffusion coefficient in this limit.

It can be seen that the two interdiffusion coefficients obtained (Eqs. (1.40) and (1.44)) - as it was expected - give the same conclusion as one can get from the bulk analogues of them: if $D'_A > D'_B$, then $D'^D \cong D'_A$ and $D'^{NP} \cong D'_B$, respectively, i.e. the GB intermixing is controlled by the

diffusivity of the faster as well as by the slower components in the Darken as well in the Nernst-Planck limit, respectively.

It is worth mentioning that a relation was derived in [40] for the composition left behind the sweeping boundary and it was obtained that

$$c_A = \alpha \frac{D'_A}{D'_A - D'_B}, \text{ with } \alpha = \frac{\frac{b_n}{\zeta}}{1+\frac{b_n}{\zeta}}. \quad (1.45)$$

In [40], the shift of the GB was interpreted as a climb of a GB step of ζ height with a GB dislocation (GBD) Burgers vector component, b_n (perpendicular to GB plane). In order to reach an order of magnitude estimation of the composition left behind the moving boundary, it was argued that for D'_A substantially larger than D'_B the $\frac{D'_A}{D'_A - D'_B}$ ratio is of order of unity and only the multiplying factor will determine the composition. Since $\frac{b_n}{\zeta}$ values were estimated to be in the order of 0.1, the experimental values were reproduced.

Recently, it was observed that there are extensive intermixing and the reactive diffusion was accompanied by grain boundary migration, grain growth, and formation of phases in nanocrystalline systems at low temperatures [19,41,42]. The explanation of general features of this low temperature reaction layer formation can be explained by the following model [19].

This model is called grain boundary diffusion-induced reaction layer formation (GBDIREAC). Indeed the GBDIREAC is similar to the DIR or DIGM. The most important difference lies in the complete ruling out the role of bulk diffusion as well as in considering the formation of new phases. This can lead to formation of a completely reacted nanocrystalline thin film into A_nB_{1-n} intermetallic layer, where n depends (if there exist more than one intermetallic phase in the phase diagram) on the initial film thicknesses and grain sizes. In fact, the details of such processes can be understood by the combination of the effect of the bimodal GB structure and the solid state reaction taking place during sweeping of the GBs perpendicular to the original boundary plane [19].

Thus instead of nucleation and growth of a product layer, parallel to the original interface, the compound phase is formed by means of GBDIREAC. High concentration regions with compositions close to the stoichiometric composition may develop in GBs and can grow perpendicularly to the GBs consuming the parent phase. The grain boundary network in thin films, even at low temperatures, is able to supply enough material to reach a complete homogenization or phase formation in the whole volume of the film. Fig. 1.11 illustrates schematically the effect of GBDIREAC on the entire composition profile inside the films. It can also be shown that the solid-state reactions can obviously start first along those GBs which were filled up earlier and the amount of the reacted phase can gradually increase and expand according to the morphology of the film [19].

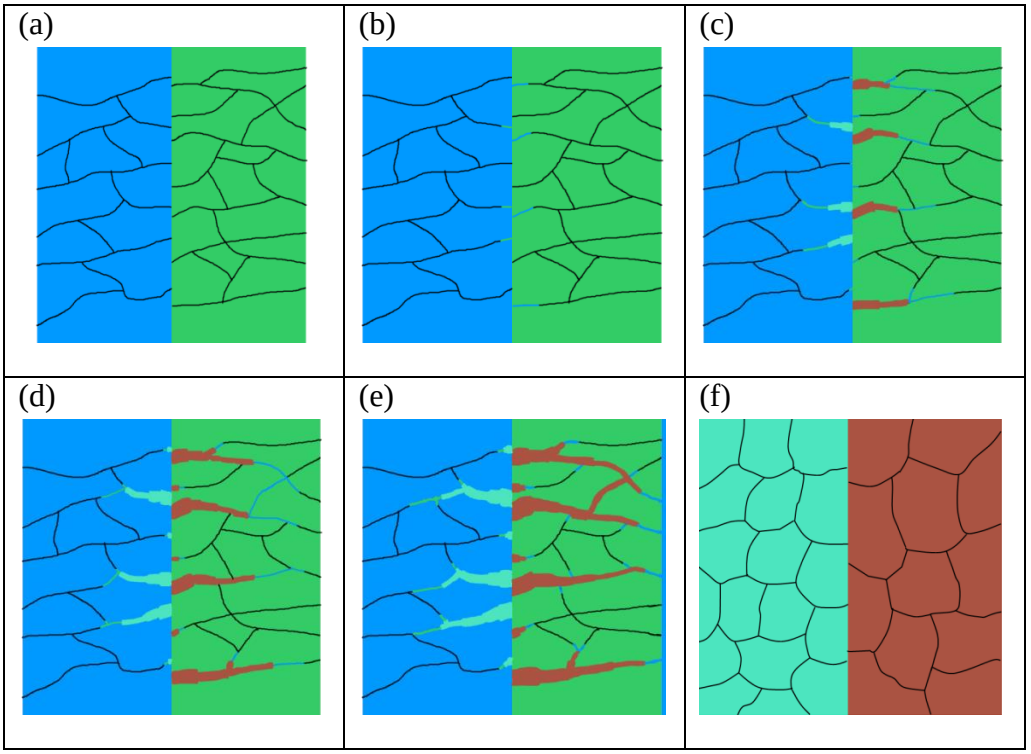

Fig. 1.11. Diffusion and formation of reaction layers around GBs in an A/B thin film, schematically. A and B are blue (dark grey) and green (light grey) and the reaction layers are light blue (lighter grey) and brown (darker grey), respectively, [19].

Chapter 2

Literature review

In this chapter, summary of the literature about Ni/Si and Ag/Au systems is presented. This highlights the importance of our topic and outlines what we will study in these systems.

2.1. Ni/Si systems

NiSi as well as its derivatives such as Ni(Pt)Si have been used extensively for contact metallization in aggressively down-scaled complementary metal-oxide-semiconductor devices, metallic source/drain MOSFETs and in the ultra-large-scale integrated circuits [43-49]. It has many advantages over the other silicides due to its lower resistivity, lower formation temperature, lower consumption of Si during the silicidation process and no resistivity increase on narrow line [44-49]. The phase diagram of Ni-Si is shown in Fig. 2.1.

A controllable formation of ultrathin metal silicide films in the sub-10 nm regime represents a chief challenge [50-53], since e.g. the scaling of CMOS devices require reproducibly obtained NiSi films in the 3-6nm regime.

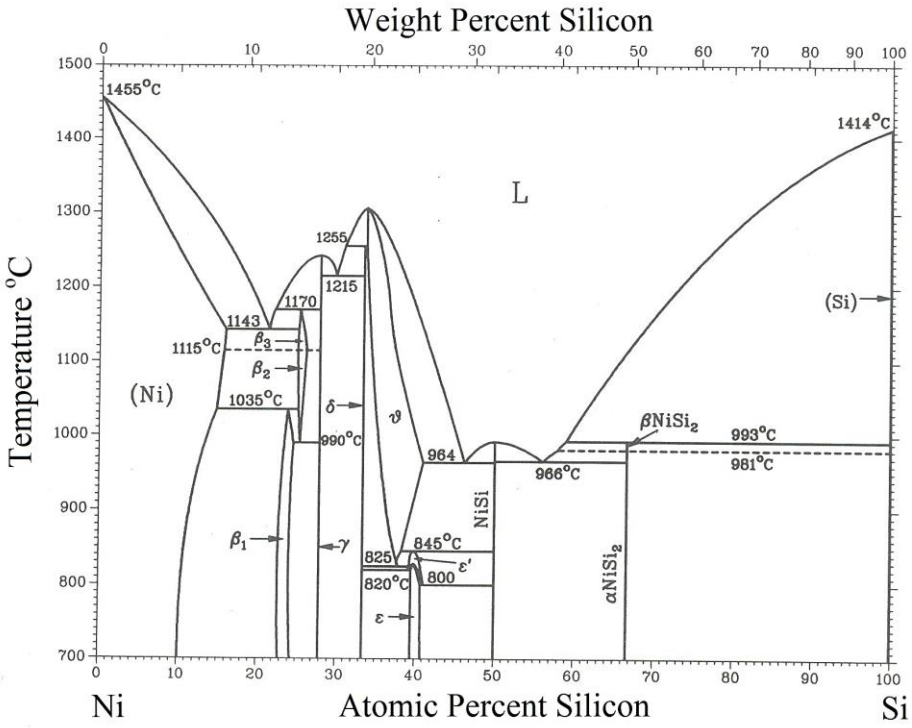

Fig. 2.1. Phase diagram of Ni-Si system [54].

The contacts based on NiSi are usually obtained by solid state reaction between Ni and Si using the self-aligned silicidation process [55,56]. The preparation of these contacts is currently done in two annealing steps. First, Ni_2Si or Ni-rich phases are formed during a heat treatment by rapid thermal annealing at 280°C (RTA1), and then the non-reacted metal is removed by selective etching. As a second step the NiSi phase is obtained after a second high temperature rapid thermal annealing at 390°C (RTA2). During annealing at high temperatures the $NiSi_2$ phase can also be formed, which is a major disadvantage for its integration in devices because of its relatively high resistivity [57].

An interesting, new process scheme was proposed recently by Zheng Zhang et al. [53], which is based on the interfacial atomic intermixing, when

a metal film is deposited on Si substrate. After the deposition of the Ni film, selective wet etching was applied to remove the deposited metal film. The silicide formation, from the left behind intermixed layer, was carried out by a rapid thermal annealing process at 500^{o}C for 5 s.

In the above high temperature technologies, the phase nucleation and formation is based on a mixed contribution of bulk and grain boundary diffusion processes during the rapid thermal annealing processes.

In this study (**Chapter 4**), we present a production scheme based exclusively on grain boundary diffusion and low temperature heat treatment. The proposed method has the following advantages; by the use of Ni_2Si, instead of Ni as the initial reaction layer, the complications related to the initial formation of sometimes non-uniform Ni_2Si layer can be avoided and the final thickness of the requested NiSi layer can be well controlled down to about 5nm thickness. In addition, the fully GB controlled process allows the use of much lower temperatures as compared to the usual RTA technologies. Thus, secondary neutral mass spectrometry (SNMS) and profilometer were used to map concentration profiles and to investigate the kinetics of solid state reactions between Ni_2Si with different thicknesses and the Si substrate at low temperatures. The microstructure of the samples was analyzed by X-ray diffraction (XRD) and transmission electron microscopy (TEM).

The trend towards smaller transistors implies thinner silicide films, whose reaction pathways are still being debated. Recent works highlight changes of phase sequence and silicide texture with the decrease of Ni thickness and the controllable formation of ultrathin metal silicide films [53,58]. Thus, nanoscale investigations of the solid state reactions as well as the better understanding of the kinetics of growth of the phases are very important. Besides, the Ni/Si system can be used as a model system for better understanding the details of the early stages of the solid state reactions at nanoscale.

In usual investigations, the thickness of the reaction layer is determined as function of the annealing time. However, the growth of a reaction layer is always a result of the *simultaneous shift of two interfaces* bordering the given phase. Thus, for a deeper understanding of such nanoscale solid state reactions, following the kinetics of both individual interfaces and the

experimental methods of their determination are very important. Knowing these, one can easily compose their combination for the interpretation of the growth kinetics of phases [59]. In previous paper of our laboratory [59], a method, based on depth profiling, was illustrated for the determination of the nanoscale shift of interfaces bordering the growing phase in Ni/amorphous-Si system. However only qualitative conclusions were drown on the growth exponents. In this study, we apply this method to investigate the effect of substrate (amorphous, a-Si, and crystalline, c-Si) as well as the addition of Pt on the kinetics of the shift of *individual* interfaces. Results obtained in Ni/a-Si, Ni(Pt)/a-Si, Ni/c-Si and Ni(Pt)/c-Si systems will be compared.

It is worth to summarize the literature data on low temperature heat treatments in Ni/c-Si and Ni/a-Si system under the condition of *unlimited supply* of silicon and nickel, which will also be the case in our studies.

a) Ni/a-Si system

- During deposition of Ni on a-Si, an amorphous nickel silicide has been formed between the nanocrystalline Ni and amorphous Si [60]. This formation is an asymmetric process, i.e. it cannot be observed at the interface obtained by deposition of amorphous Si on Ni [61]. This is due to the so-called dynamic segregation effect: the Si segregates on the surface of Ni and thus during the deposition, the formation of an intermixed layer is possible if Ni is deposited on the surface of a-Si, but not by deposition of Si on Ni. The above intermediate (amorphous) layer is a mixed zone containing regions corresponding to both NiSi and Ni_2Si compositions (see Fig. 4 in [61]).

- During low temperature heat treatments (between 187^{o}C and 217^{o}C), a crystalline Ni_2Si layer forms between the Ni and the amorphous nickel silicide [60]. The composition of the latter is now about one Ni to one Si atom (see Fig. 6 in [60]). The two phases (the amorphous silicide and the crystalline Ni_2Si) simultaneously grew further. It was also concluded in [60] that nucleation barriers are responsible for the initial formation of the amorphous nickel silicide, and the formation of the Ni_2Si cannot be explained by a pure planar-growth mechanism. After longer annealing times, crystalline Ni_2Si and NiSi phases grew. On the other hand it was shown in [62], from in situ TEM and X-ray diffraction in Ni/a-Si

multilayers, that after annealing at 400^{o}C for 6h, an amorphous silicide phase has been formed at the Ni/a-Si interfaces according to a planar growth mode. TEM observations also confirmed that amorphous silicide has been formed along the Ni grain boundaries too.

- In [63], the authors also observed that two different phases (Ni_2Si and NiSi) have been formed in two distinct layers and the growth of these phases was parabolic with activation energy in the range of 1.3-1.6 eV. These activation energies suggest that the growth of the reaction layers is controlled by grain boundary diffusion [64] of Ni along silicide grain boundaries. As it was proposed in [64], such growth mechanism can be imagined e.g. as the fast diffusion of Ni along the Ni_2Si grain boundaries and a subsequent interface diffusion along the interface between the Ni_2Si and Si-rich region (see also Fig. 6c in [64]).

- Regarding the growth mode, in a more recent paper [65] – using differential scanning calorimetry (DCS) and in-situ XRD – it was shown that the growth of *crystalline* Ni_2Si (the XRD did not give information about the amorphous phase if it was present) could be described by a linear parabolic law at 210^{o}C i.e. the first stage of the growth was linear, which is in line with the conclusion of [60] (non-planar growth mode).

b) Ni/c-Si system

There is unanimous opinion in the literature (see e.g. [63,66,67]) that only (strained) Ni_2Si forms at low temperatures (200-327 ^{o}C) and grows as an intermediate layer between the Ni and Si. Its growth is diffusion limited with activation energy of about 1.5 eV indicating the Ni grain boundary diffusion along the Ni_2Si grain boundaries as the main mechanism. Note that in [67] it was established that a composition gradient existed inside the Ni_2Si layer but its quantitative estimation was difficult (it was about 3-15% along the growing layer). This is in accordance with the conclusion, drawn in [66], that a transient phase (identified as Ni_3Si_2) just after the Ni_2Si formation can be present. From TEM observations it was concluded that this phase was nonuniform.

c) Effect of Pt additions

In addition to the above observations, there are many publications in the literature about the effect of Pt addition on the first phase formed as well as on the stability of NiSi, as compared to the Ni_2Si [68-72]. It was observed that the formation of silicides began during the deposition and there were two regions with composition corresponding to Ni_2Si and NiSi. While the NiSi product formed a continuous layer with a relatively constant thickness, the Ni_2Si particles formed seeds and grew laterally. Furthermore, it was argued that after the relaxation of stresses accompanied to the formation of the Ni_2Si phase, the fast growth of the NiSi occurred [69]. These results, as compared to those obtained in systems without Pt, were interpreted by the very low solubility of Pt in the bulk of Ni_2Si (as compared to the NiSi) and segregation at the grain boundaries: this slows down the silicide growth kinetics.

2.2. Ag/Au system

It is well known that during interdiffusion in binary AB systems at low temperatures, where the bulk diffusion is completely frozen out, the inequality of the grain boundary, GB, diffusion fluxes can lead to diffusion induced grain boundary migration, DIGM, and/or grain boundary diffusion induced recrystallization, DIR, [28,38,40,73]. At the same time, the above inequality, similarly as in the case of bulk intermixing, can lead to porosity formation at GBs of the faster component due to the resultant GB vacancy flow. Although there are evidences for vacancy mechanism of GB diffusion (see e.g. [20,74,75]), there are only few experimental results on porosity formation along GBs as the consequence of GB intermixing. In [76], beside the observation of DIGM and DIR in Cu/Ni diffusion couple, pore formation along the GBs was observed by TEM on the Cu side after different heat treatments between 600 and 900^{o}C. In [77], some porosity was observed in the AlNi matrix at the vicinity of wedge-type shape Cu enriched penetration zones by optical microscopy after heat treatment at 850^{o}C for 54 hours. The authors interpreted this as the result of GB diffusion intermixing between Cu and Al (assuming that the Cu preferentially occupied sites in Al-sublattice, i.e. the process could be considered as a quasi-binary intermixing). In both above cases, the porosity formation was observed on micrometre scale and the annealing temperature was relatively high, i.e. the contribution of bulk diffusion was not negligible: in [77] even it was concluded that their

experimental conditions corresponded to B-regime (instead of C-regime) of GB diffusion.

In this study (chapter 4), we provide clear experimental evidence on porosity formation along GBs and triple junctions in Ag during intermixing in nanocrystalline Ag(15nm)/Au(15nm) thin film at low temperature (at 150^{o}C) where the bulk diffusion processes are completely frozen out. In addition, it was shown in [13] and [78] that the application of small hydrostatic pressure (at about 180 bar: low enough that the pressure dependence of the bulk diffusion coefficients can be neglected) led to disappearance of the pores formed in the bulk of Cu of the Cu/Ni diffusion couple. Thus, following the plausible analogy between the bulk and GB intermixing, we show that the application of small (about 100 bar) hydrostatic pressure is enough to prohibit the nanoscale porosity formation along GBs at 150^{o}C. In addition, we demonstrate that homogenization is possible by DIGM in both nanocrystalline Ag and Au films, at least up to the level corresponding to the compositions left behind the moving boundaries in their wakes.

Chapter 3

Experimental techniques & tools

Different thin film systems such as Ni_2Si/c-Si, Ni/c-Si, Ni/a-Si, Ni(Pt)/c-Si, Ni(Pt)/a-Si and Ag/Au were deposited by DC magnetron sputtering. The sputtering rates were calculated from the layer thickness measured by AMBIOS XP-1 profilometer. The samples were annealed in vacuum furnace (10^{-7} mbar) at different temperatures for different annealing times. Ag/Au samples were annealed under high and low hydrostatic pressure of high purity Ar.

Structure of some of the samples was investigated using X-ray diffraction and by transmission electron microscope. The concentration-depth profiles were determined by means of secondary neutral mass spectrometry and profilometer. The resistance of the Ni_2Si/c-Si sample as function of the annealing time was measured by the 4-wire resistance measurement technique at 180^oC.

3.1. DC Magnetron Sputtering

The DC magnetron sputtering system consists of power supply, low pressure noble gas (Ar), two electrodes and a magnet inside a chamber (see Fig. 3.1). The target is placed at the cathode while the substrate is placed at the anode. Applying DC voltage accelerates free electrons in the chamber. These free electrons collide with the Ar atoms leading to ionization of Ar atoms (formation of plasma). The positive Ar ions will be accelerated

towards the target and bombard (sputter) the target. The magnet is placed below the target to increase the electrons participating in the ionization and to make the electron orbits curved leading to more collisions. This increases the sputtering rate, decreases the voltage required to strike the plasma and reduce the substrate heating from the electron bombardment.

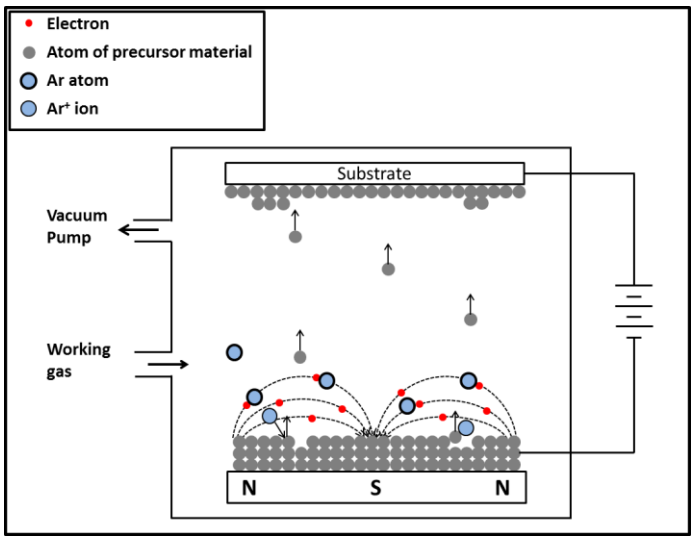

Fig. 3.1. DC magnetron sputtering system, schematically.

In our DC magnetron sputtering system (see Fig. 3.2), three targets with three magnetrons can be used simultaneously. Each target is shielded with shutter. The magnetrons are fixed on the bottom of a stainless steel chamber. Transition of the sample between the targets and controlling the shutters can be done manually or automatically with computer program. Also, the chamber contains vacuum gauges, gas management, quartz crystal monitor and an in-situ heating sample holder attached with an annealing system. The distance between the target and the sample holder is 5 cm. The targets are disc-shaped with diameter of 2 inch. The homogeneous area of the deposition is about 2-3 cm^2, thus limited number of samples could be prepared in one deposition circle.

Before the sputtering process, the chamber was pumped down to a high vacuum (~10^{-7} mbar). This base pressure is achieved by the combination of a turbo-molecular pump and a rotary pump. During the sputtering process, high purity (99.999%) Ar gas is introduced into the chamber. The Ar pressure is maintained $5x10^{-3}$ mbar under dynamic flow. Then, the plasma was created by applying DC voltage to the target. The sputtering power was 20 and 40 W. The ions of the plasma will bombard the atoms of the target surface. These atoms will move further toward the substrate.

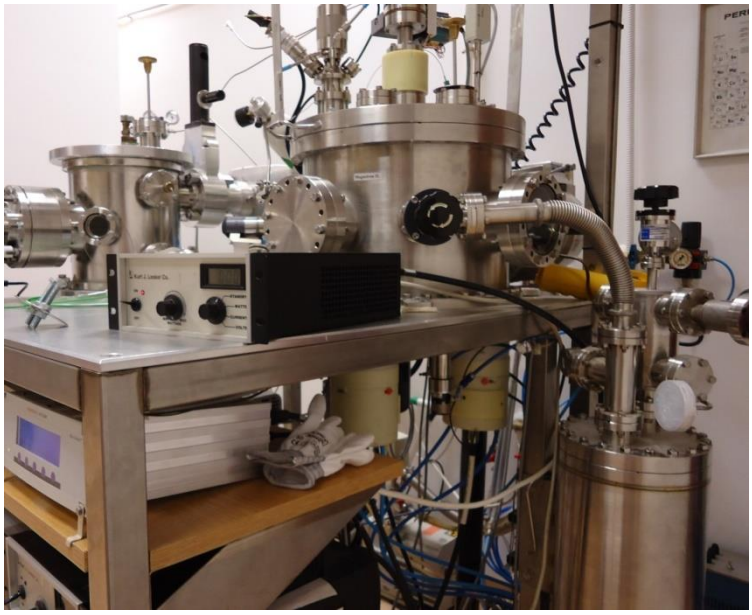

Fig. 3.2. The side view photograph of the DC magnetron sputtering system.

In order to determine the sputtering rates, films of each target were deposited for certain time and their thicknesses were measured by profilometer (see section 3.4). The thin film systems were deposited at room temperature.

Before introducing the SiO_2 and the single crystal-Si substrates into the sputtering system, the substrates were cleaned in distilled water and later with ethanol in ultrasonic bath to get rid of dust and any other surface contaminants. The c-Si substrate was etched by HF to remove the oxides and nitrites. The samples for top-view TEM were prepared as follows: instead of

using SiO_2 substrate, the bilayer was deposited on a freshly cleaved single crystalline sodium chloride surface. After annealing, the substrate was dissolved and top-view TEM images were made.

3.2. High vacuum and hydrostatic pressure furnaces

The samples were annealed at low temperatures for different annealing times. Most of samples were annealed in high vacuum (~10^{-7} mbar) furnace (see Fig. 3.3). This furnace has movable sample holder and shutter to decrease the heating and cooling times to be suitable for short annealing times.

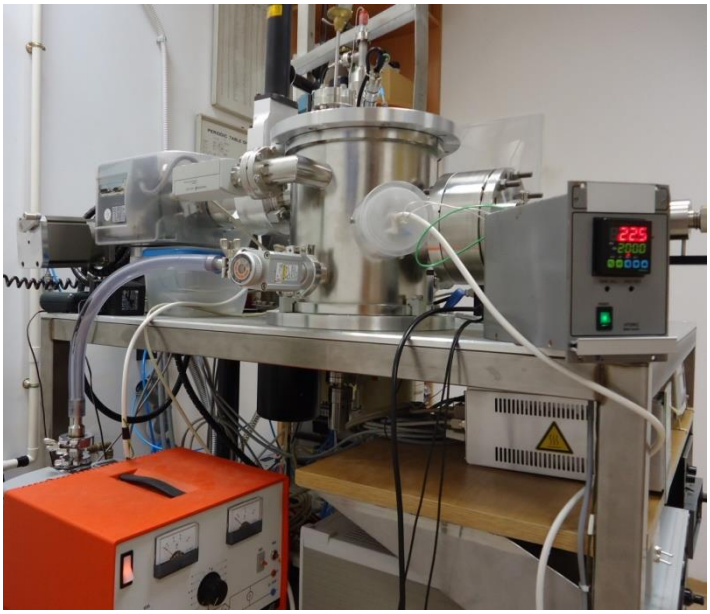

Fig. 3.3. The side view photograph of the high vacuum furnace.

The Ag/Au samples were annealed in hydrostatic pressure furnace (see Fig. 3.4). First, the furnace was pumped down to 10^{-2} mbar using rotary pump. Then, high purity (99.999%) Ar gas is introduced into the furnace and the furnace was pumped down two times to clean the furnace. Finally, the low (1 bar) or high (100 bar) pressure of Ar are introduced in the furnace during the annealing.

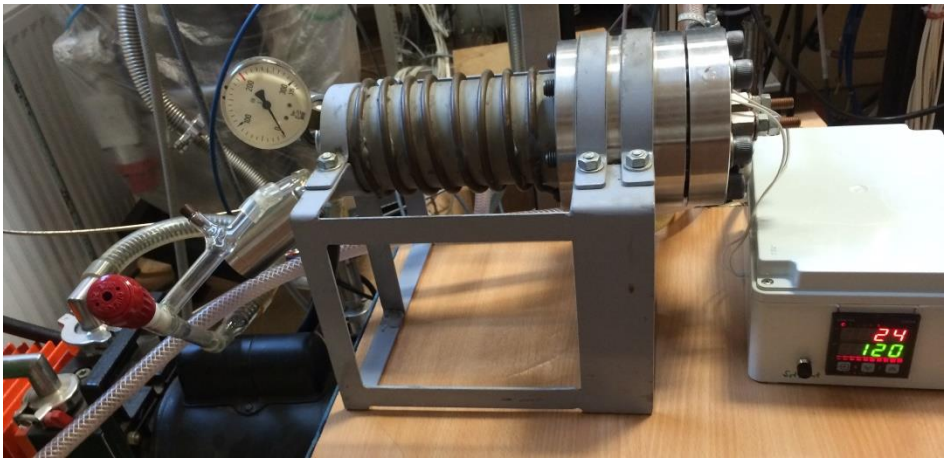

Fig. 3.4. The side view photograph of the hydrostatic pressure furnace.

3.3. Secondary Neutral Mass Spectrometry (SNMS)

The depth profiles of the samples have been investigated by means of secondary neutral mass spectrometer (SNMS) (INA-X, SPECS GmbH, Berlin) equipment [79] (see Fig. 3.5). In SNMS, the sample is destructively analyzed by layer-by-layer removal of the material. An ion beam successively erodes the material, while the ejected neutral atoms are post-ionized and analyzed in a quadruple mass spectrometer [80]. The ion bombardment and the latter post-ionization are achieved by the low pressure Ar gas plasma [1]. SNMS has an extremely high lateral homogeneity: low bombarding energies (about 300 eV) and homogeneous plasma profile result in an outstanding depth resolution (<2 nm) [81] and the detection limit is about 10 ppm [81,82].

SNMS is suitable to investigate conducting and non-conducting samples. The latter one is provided by High Frequency Mode, which controls the amount of charge being transferred to the sample by periodically interrupting ion accelerating voltage between the sample and the plasma. Thus, the charging of the sample can be compensated [1].

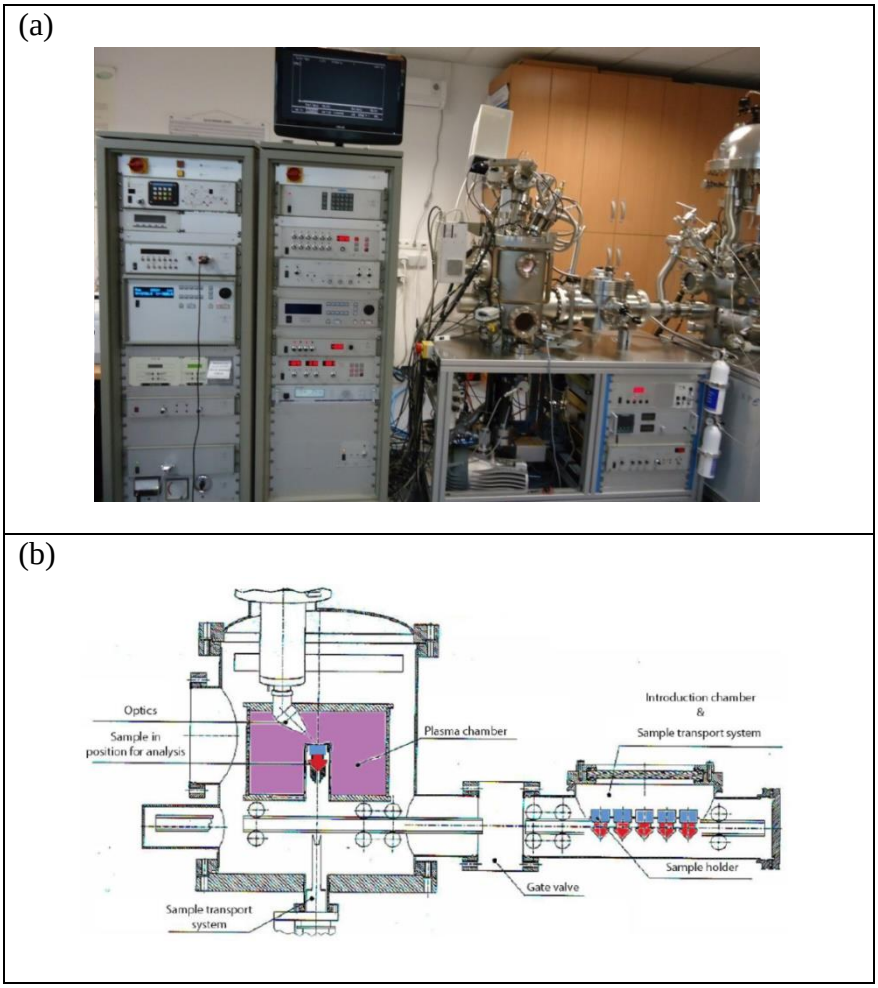

Fig. 3.5. The INA-X Secondary Neutral Mass Spectrometry system; (a) side view photograph, (b) schematic view [1].

Using this system, the structure and stability of thin films and the development of grain boundary diffusion and interface reactions as well can be followed in nanometer depth resolution. This technique provides relatively fast results since it does not require special sample preparation. However, many samples may be required for certain investigation since it is destructive technique.

Certain mask with circular hole should be placed on the top of the investigated sample. In our case, Cu mask was used and the diameter of the

hole in the center of the mask was 2mm. SNMS provides intensity-sputtering time profiles which are required to be converted to composition-depth profiles. The intensity is converted to composition by determining/knowing the sensitivity factors of the investigated elements. The sputtering time is converted to depth by measuring the depth of the sputtered craters at different points of the measurement by the profilometer (see section 3.4) and by using the proportionality between the intensity and the number of sputtered particles [83]. Before the conversion, the background of the plasma is subtracted from the intensity.

3.4. Profilometer

The thickness of the films was measured by Ambios XP-1 profilometer (see Fig. 3.6). Also, it was used to determine the sputtering rates of the different elements used in this study (W, Ni_2Si, Ni, Si, Au, Ag). Furthermore, it was used to measure the depth of sputtered craters at different points to convert the sputtering time axis (of the intensity-sputtering time profile) into depth. In this contact profilometer, a stylus with ~2 μm radius moves along a certain path on the sample to follow the changes of the surface. The system is able to measure/identify the small surface variations or steps, layer thicknesses or the roughness of the surface. We used low-force stylus (0.05-10 mg) to avoid the scratching/damaging. This technique can be used with large variety of samples.

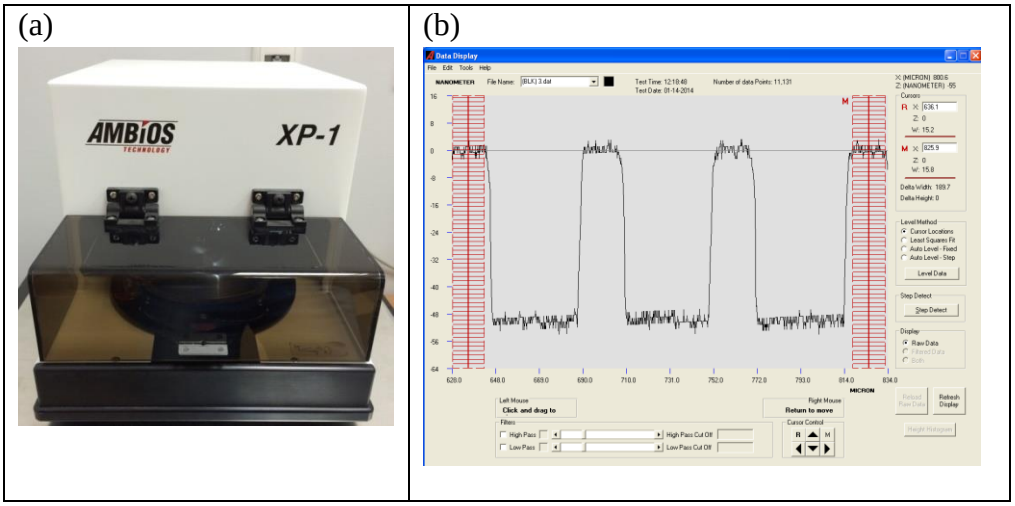

Fig. 3.6.(a) Ambios XP-1 profilometer, (b) a measured depth profile.

3.5. X-ray Diffraction (XRD)

The diffraction phenomenon is observed when a wave meets an object having a periodicity similar in length. Since the wavelengths of X-ray are in the same order of magnitude as the distances of atoms in matter, X-ray can provide information about the crystalline structure through diffraction patterns that follow the fundamental Bragg's law:

$$2d \sin\theta = n\lambda \tag{3.1}$$

where d is the distance of the lattices planes in crystalline structures, θ is the incident angle and λ is the wavelength of the wave beam.

In our study, we used Philips X-ray diffractometer (model X'-Pert) by utilizing monochromatic CuK_α radiation operated at 40 kV and 25 mA to study the Ni_2Si/Si and Ni/Si systems.

3.6. Transmission Electron Microscope (TEM)

The microstructure of samples was analyzed by transmission electron microscope (TEM) (JEOL2000FX+EDS). TEM was used for both the top-view and cross-section view of the samples. TEM provides both a direct image and a diffraction pattern of the specimen. In this technique, high-energy electrons are used as probe. Imaging of the transmitted electrons reveals information on the morphology and structure of the sample. Furthermore, the energy analysis of the transmitted electrons or the emitted characteristic X-rays provide information on the chemical composition. The main disadvantage of TEM is that the sample suffers from many heat treatments during the preparation for cross-sectional TEM. This may affect the microstructure of the sample to be analyzed. The description of theory and practice of TEM techniques can be found in [84].

Chapter 4

Results and discussion

In this chapter, I show the results and detailed discussion of the diffusion and solid state reactions at relatively low temperatures in Ni_2Si/c-Si, Ni/Si and Ag/Au thin film systems.

4.1. Production of NiSi phase by grain boundary diffusion induced solid state reaction between Ni_2Si and Si(100) substrate

Fig. 4.1 shows the concentration-depth profiles of the as-deposited and annealed samples of W(10nm)/Ni_2Si(20nm)/c-Si at 180^oC for different annealing times. The symbols are just for identification of curves, since the intensity/sputtering time profiles were recorded continuously. The W layer was used just to avoid the surface oxidation of the samples measured by the SNMS, since we find that it makes difficulties in the calculations during the conversion from intensity to concentration. It is clear that the as-deposited Ni_2Si film is homogeneous and the annealing leads to diffusion of Si into the Ni_2Si layer. With increasing the time of annealing, the film is still Ni rich until 1 h, while homogenous NiSi is formed after 2-3 h. It is obvious that there is no clear formation of planar reacted layer at the initial interface, which would be expected for a "normal (i.e. bulk diffusion assisted) growth".

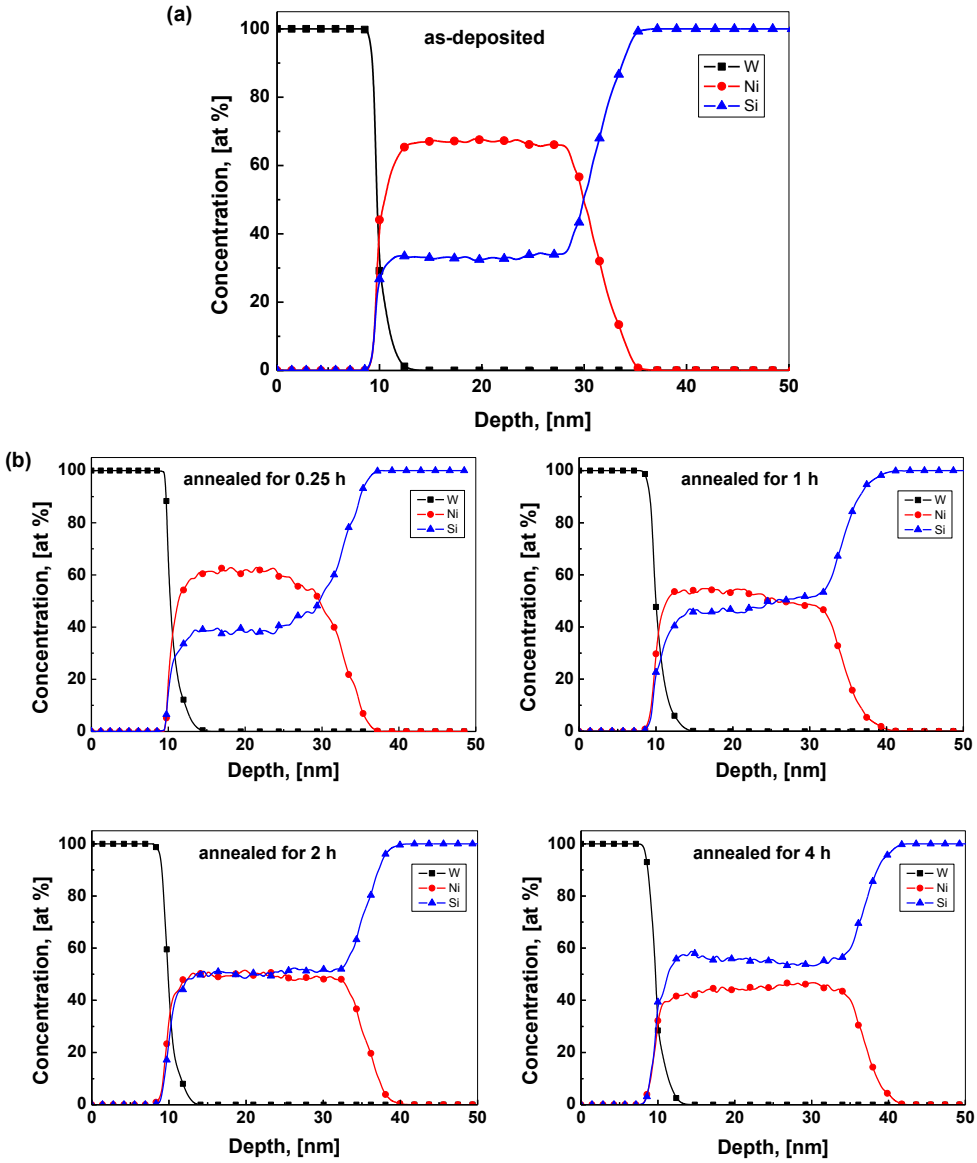

Fig. 4.1. Concentration-depth profiles of W(10nm)/Ni_2Si(20nm)/c-Si; (a) as-deposited, (b) annealed at 180^{o}C.

Top view X-ray diffraction pattern (XRD) of the as-deposited and annealed Ni_2Si/c-Si samples at 180^{o}C for 2 h is shown in Fig. 4.2, confirming the phase transformation from Ni_2Si to NiSi. The crystallite size

d_o of the as-deposited Ni_2Si film was estimated from the full width at half maximum (FWHM) of the (021) peak using Debye–Scherrer formula [85]:

$$d_o = \frac{0.9\,\lambda'}{\beta\,\cos\theta} \tag{4.1}$$

where β is the FWHM (0.44°), λ' is the wavelength of CuK_α radiation and θ is the angle of diffraction: $d_o \cong 20nm$. It is worth noting that in the freshly sputtered film no X-ray reflection peaks were observed, i.e, the film was X-ray amorphous: the "as-deposited" spectra, shown in Fig. 4.2, was obtained after about two months ageing at room temperature. Keeping the as-deposited samples at room temperature could cause partial recrystallization but no other changes (regarding the phase transformation) are expected. This recrystallization could be achieved during the heating up to the annealing temperature. All the heat treatments were done on freshly prepared samples.

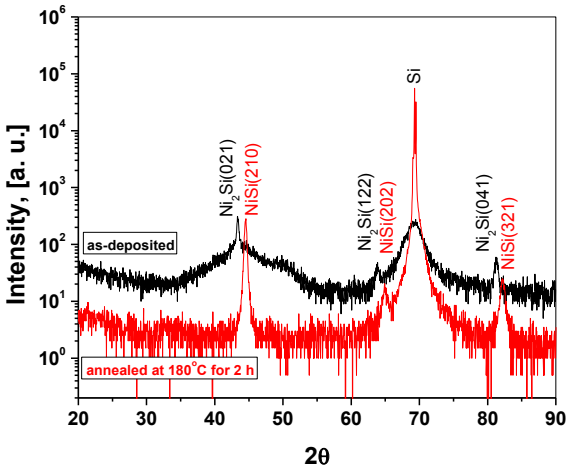

Fig. 4.2. XRD of as-deposited and annealed Ni_2Si/c-Si samples at 180°C for 2 h.

For further investigations, the W(10nm)/Ni_2Si(20nm)/c-Si samples were annealed at 190 and 200°C for different annealing times. The concentration-depth profiles are plotted in Fig. 4.3(a and b). It can be seen that the NiSi phase was formed after 1 and 0.5 h for the samples annealed at 190 and 200°C, respectively. At longer times (i.e. in over-aged states: 2 and

1h for 190 and 200°C, respectively) surprisingly there are steps suggesting the formation of the $NiSi_2$ not near to the Si, but near to the W.

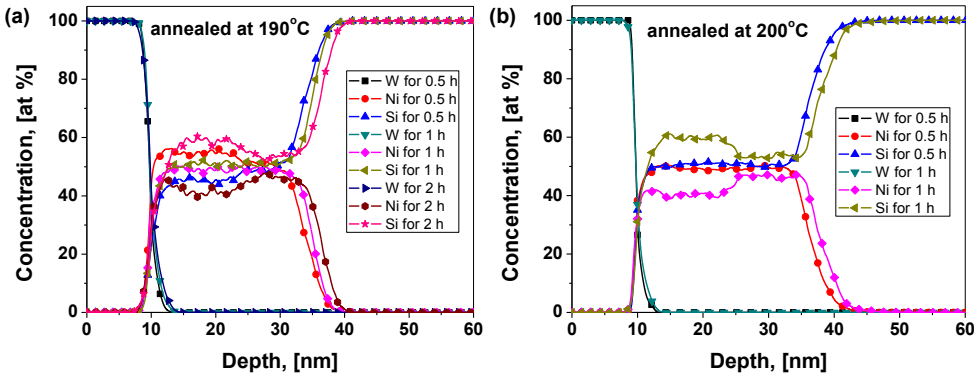

Fig. 4.3. Concentration-depth profiles of W(10nm)/Ni_2Si(20nm)/c-Si annealed for different annealing times; (a) 190°C, (b) 200°C.

To investigate the solid state reactions at lower thicknesses, samples with 10 and 5 nm thick Ni_2Si were annealed at 180°C for different times. The concentration-depth profiles obtained are shown in Fig. 4.4(a and b). It can be seen that the NiSi phase was formed at 1 and 0.25 h for the samples with Ni_2Si thicknesses of 10 and 5 nm, respectively. At 0.5 h already the increased Si content (see especially the shoulder close to the Si in Fig 4.4(b)) indicates that the formation of $NiSi_2$ takes place too.

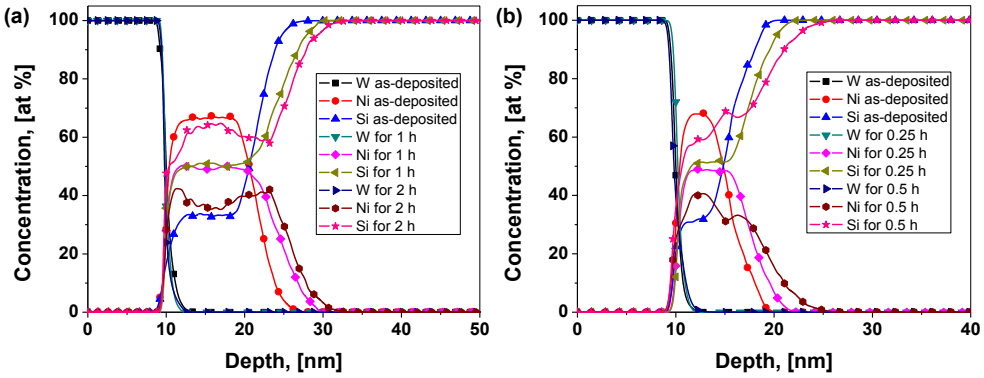

Fig. 4.4. Concentration-depth profiles of as-deposited and annealed samples for different annealing times at 180°C; (a) W(10nm)/Ni_2Si(10nm)/c-Si, (b) W(10nm)/Ni_2Si(5nm)/c-Si.

From Figs. 4.1, 4.3, 4.4, we can construct the temperature-time and thickness-time windows inside of which the formation of NiSi takes place (see Fig. 4.5(a and b)).

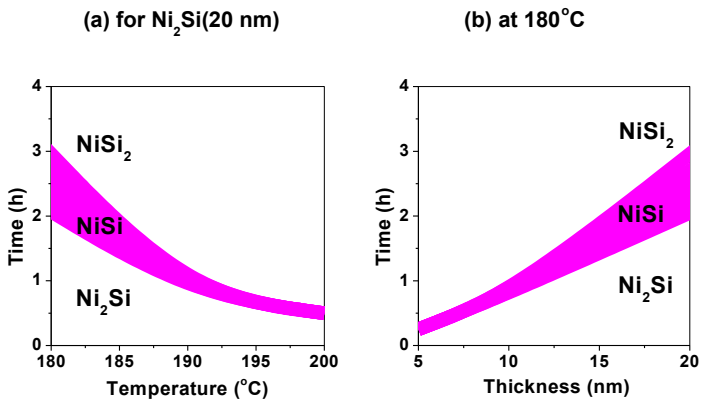

Fig. 4.5. (a) Temperature-time and (b) thickness-time windows for the formation of NiSi.

As we already mentioned, the formation of the NiSi phase – instead of nucleating at the original Ni_2Si/Si interface and growing as a compact planar layer with parallel phase boundaries – shows an anomalous growth process. Indeed Figs. 4.1, 4.3, 4.4 illustrate that the most important change is the gradual increase of the Si content inside the original Ni_2Si layer until the composition here corresponds to the NiSi phase. Since at these low temperatures, the bulk diffusivity of the Ni in the Ni_2Si after 1 hour at 200°C would allow of about 1.4×10^{-4} nm bulk penetration depth [86] only (and the Si bulk diffusivity is at least two orders of magnitude less than that of Ni) [86], the contribution of the bulk diffusion to this reaction can be definitely excluded. Thus the grain boundary, GB, diffusion should be the determining process.

It is known that at low temperatures, a complete intermixing of components in binary nanocrystalline couples can happen (called also as "cold homogenization") [87]. This can take place by GB diffusion induced boundary migrations through the volume [19,22,24,42,87,88]. Even it was shown that the alloyed zones left behind by the moving boundary can be not

only solid solutions but ordered phases as well [19,30,31,42,89-91]. Such type of low temperature reaction product formation is also called as grain boundary diffusion induced reaction layer formation (GBDIREAC) [19].

It is more and more widely accepted that in both processes, at intermediate temperatures, the driving forces are related to stress accumulation and relaxation ahead/around the moving boundary [22,28]. In case of low temperature processes (when there is no volume diffusion ahead of the migrating GB), it is most likely that the driving force is the diffusion induced GB stresses (created by the differences of the GB atomic fluxes of the two components) [92]. Furthermore, in references [93] and [94] expressions were given for the front velocity as function of the average migration distance, L, and it was found that it can be constant for small L values. Since in those investigations the typical migration distances were in the order of 0.1-1 microns, it can be assumed that a linear regime can be observed in our nanoscale experiments. Furthermore, Pan and Balluffi [95] constructed the $L(t)$ function from the time dependence of the concentration of the plateau region. This idea can also be applied here.

It is worth mentioning that a closer look of the composition profiles between 0.25 and 2 h in Fig. 4.1 reveals that, simultaneously with the overall increase of the Si composition in the layer, there is a small step in the Si composition near to the Si substrate, which gradually diminishes with increasing time. This can be the effect of DIR: nearby the original interface the stress accumulation can be strong enough to initiate the formation of small new grains with NiSi composition, similarly as e.g. it was observed in Au/Cu system [31]. Indeed, it was obtained in [31] by TEM that new grains were formed in the reaction zone. Fig. 4.6 shows the cross sectional TEM for the as-deposited sample. As during even a very careful preparation, the sample more or less suffers a warming up, this “as received” sample is equivalent to a certain intermediate stage of annealing (e.g. to 20nm thick annealed sample for about 0.25-1 h at 180^{o}C). It can be seen that in the vicinity of the Si layer the grain size is much less than far from it. Of course the above explanation is one of the possible explanations for the morphology of the reaction and more extended TEM would be necessary to reveal the details.

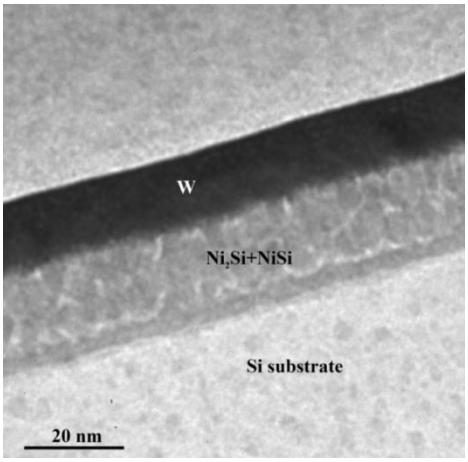

Fig. 4.6. TEM picture of the as-deposited W(10nm)/Ni_2Si(20nm)/c-Si sample.

In Fig. 4.7, on the basis of our observations summarized above, we show a schematic view of the time evolution of the process.

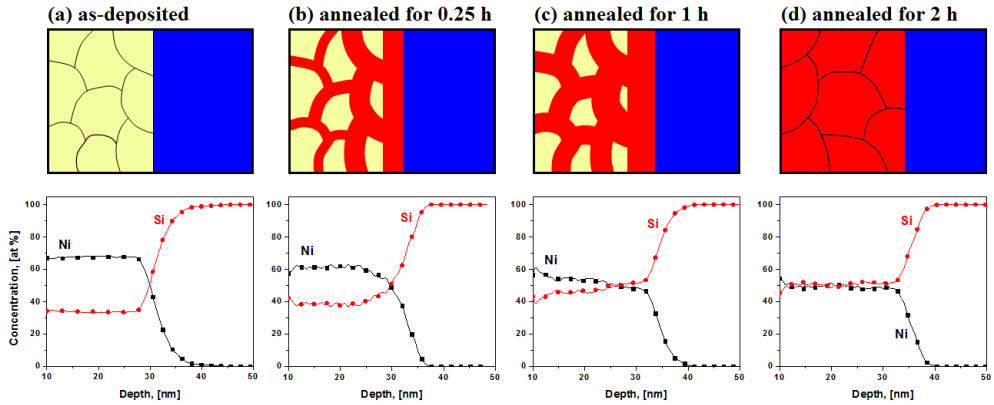

Fig. 4.7. Sketch of grain boundary diffusion of Si (blue) into Ni_2Si film (yellow) forming NiSi (red), for as-deposited and annealed samples at 180°C.

Let us turn back to the increase of the average composition and its relation to the interface velocity. In the following we will neglect the small morphological difference and the film will be taken to have a homogeneous distribution of grains. Since in thin films the average grain size, d_o, is usually less than the film thickness, H, it is plausible to assume spherical

grain structure with $\delta/2$ thick spherical shell (see Fig. 4.8) at the beginning (at $t = 0$). As a first step, the GBs will be filled up (during t_o time) and then the interface shift of this GB phase starts by a constant interface velocity, v. We assume that the interface shift starts after the Ni_2Si GBs have been filled up to the equilibrium composition of the new phase. Then the internal sphere, in which the initial composition is c_o, has the radius $d/2 = d_o/2 - (\delta/2 + vt')$, if d is the diameter and $t' = t - t_o$. Now, denoting the equilibrium Si composition of the growing phase by c_e, the average concentration, c, in the middle of the film can be given as:

$$c = \left(\frac{d}{d_o}\right)^3 c_o + \left(1 - \left(\frac{d}{d_o}\right)^3\right) c_e$$

$$= c_o + \frac{(c_e - c_o)6\left(\frac{\delta}{2} + vt'\right)}{d_o} + \frac{(c_o - c_e)12\left(\frac{\delta}{2} + vt\prime\right)^2}{{d_0}^2}\left[1 - \frac{(\delta + 2vt\prime)}{3d_o}\right], \qquad (4.2)$$

which, with $c_e = 1/2$ and $c_o = 1/3$ and neglecting terms $(\delta + 2vt')/d_o$ on the third power, has the form

$$\frac{c}{c_e} = \frac{2}{3} + \frac{\delta}{d_o}\left(1 - \frac{\delta}{d_o}\right) + \frac{2vt'}{d_o}\left(1 - \frac{2\delta}{d_o} - \frac{2vt'}{d_o}\right). \qquad (4.3)$$

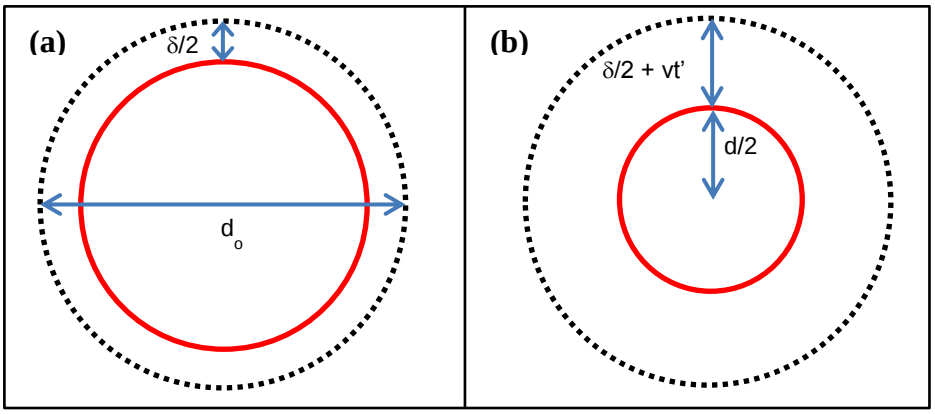

Fig. 4.8. Reacted and un-reacted zones in a spherical grain just after the saturation of the GB of δ thick (a) and after some additional heat treatment when the interface moves with velocity v (b), schematically.

At short times, the last term in the last bracket of Eq. (4.3) can be neglected leading to linear relation. Fig. 4.9 shows the average composition

inside the silicide layer as function of the annealing time, t: the first part is linear (the saturation at longer t values is due to finite size effects). From the intercept of the linear initial part, $\delta/d_o = 0.07$ can be obtained (by assuming that the t_o time necessary to start the interface shift is negligible) which, with $\delta = 0.5nm$, yields $d_o = 7nm$. The 7nm grain size is less than that obtained with the XRD data: $d_o = 20nm$, but taking into account the errors in both estimations the agreement is still acceptable (as an order of magnitude agreement). Using $d_o = 7nm$, the velocity of the interface shift is $2\text{x}10^{-4}$ nm/s.

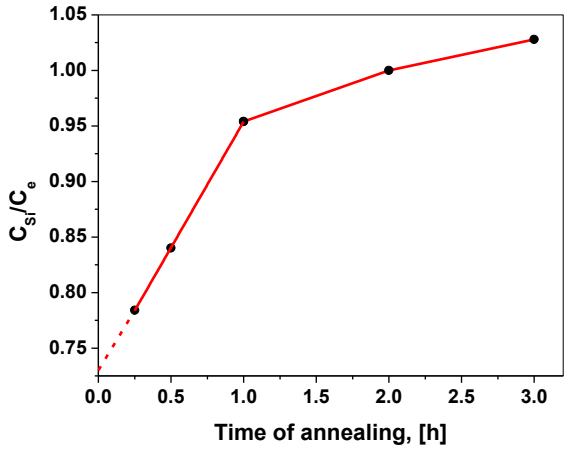

Fig. 4.9. Dependence of the average concentration of Si, c_{Si}/c_e, on the annealing time at 180°C for 20 nm thick initial Ni_2Si layer.

Usually the growth process of silicides is divided into two regimes: formation or nucleation and growth regimes [96-98]. The activation energy, Q_g, of growth constants, K_g, for the parabolic growth of Ni_2Si, was equal to the activation energy of the GB diffusion of the Ni (the faster component) indicating that the GB diffusion should have important contribution [86,97], even at higher temperatures than those used by us. In the formation regimes, the nucleation and lateral growth of the nuclei takes place. The picture is much more puzzling and sometimes even linear growth was observed: this is why sometimes it is called reaction rate control regime. Thus, the analysis of

experimental data is frequently carried out by the so-called linear-parabolic growth law giving a unified description for the linear and parabolic regimes. Although there were indications in the literature [65,96-99] that the nuclei can be formed and grow not only at the original interface but also e.g. at triple junctions of GBs, in general not too much attention was given to understand the linear dependence [97]. It is important mentioning that using experimental techniques in which only the amount of the product phase is detected as the function of the time (e.g. X-ray diffraction, electrical resistivity, etc.) one cannot know about where the new phase forms and how it grows.

Our results offer a plausible explanation for the linear growth kinetics in this regime at low temperatures: if the front velocity is constant, the amount of the product phase should grow linearly with time and the activation energy obtained from this part should be close to the activation energy of GB diffusion. This can also explain why the activation energy, Q_f, obtained from the temperature dependence of linear growth constant, K_f, (in $x = K_f t$) is little bit less than Q_g [65]. In contrast, according to the reaction rate control, it is expected that $Q_f > Q_g$ [65,97-99].

Since in the traditional technology the Pt addition is used just to stabilize the NiSi phase (as compared to the other two, Ni_2Si and $NiSi_2$, possible phases), we also checked the role of Pt addition on the process introduced here. Fig. 4.10 shows the effect of 5% Pt addition on the formation process. It can be seen that surprisingly the Pt slows down the NiSi formation process and the $NiSi_2$ phase (shoulder in the Si side) appears after 3h annealing before the formation of the homogeneous NiSi layer finished. Thus, it can be concluded that our process scheme does not need Pt addition; even its presence leads to some negative effects.

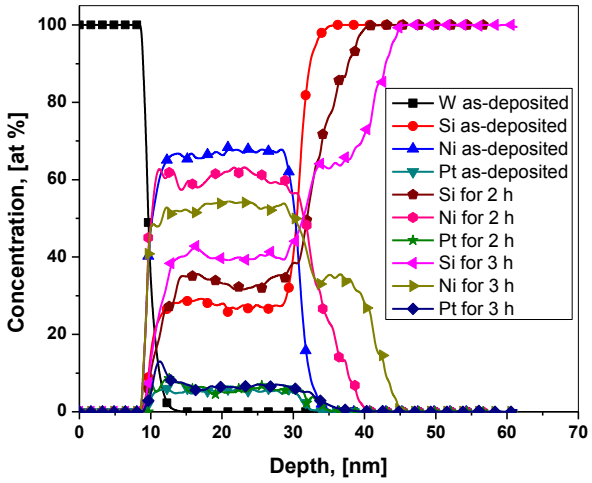

Fig. 4.10. Concentration-depth profiles of W(10nm)/Ni_2Si(20nm)Pt(5%)/c-Si; as-deposited and annealed at 200^{o}C for different annealing times.

The resistance of the film with 20 nm thick Ni_2Si layer was also measured versus the annealing time at 180^{o}C. It is clear from Fig. 4.11(a) that the resistance, after the sample reached the annealing temperature, decreases with increasing annealing time. In [100], a relation for the conductivity of a matrix (index 1) containing spherical particles of the second phase (index 2) was derived:

$$\frac{\left(\frac{k}{k_1}-1\right)}{\left(\frac{k}{k_1}+2\right)} = \rho^* \frac{\left(\frac{k_2}{k_1}-1\right)}{\left(\frac{k_2}{k_1}+2\right)}. \qquad (4.4)$$

Here ρ^* is the volume fraction of the embedded spherical particles into the matrix ($\rho^* = V_2/(V_1+V_2)$), k is the conductivity of the two phase materials, k_1 and k_2 belong to the matrix and to the second phase, respectively. Let us denote the volume of Ni_2Si by V_2 and that of NiSi by V_1 (i.e. the Ni_2Si phase corresponds to the spherical particles and the shell is the NiSi phase) and thus $\rho^* = 1$ at $t = 0$ and $\rho^* = 0$ at $t = \infty$, since at $t = 0$, $k/k_1 = k_2/k_1$ and at $t = \infty$, $k/k_1 = 1$. Thus, ρ^* is a monotonic decreasing function of the time between $t = 0$ and $t = \infty$, changing between 1 and 0.

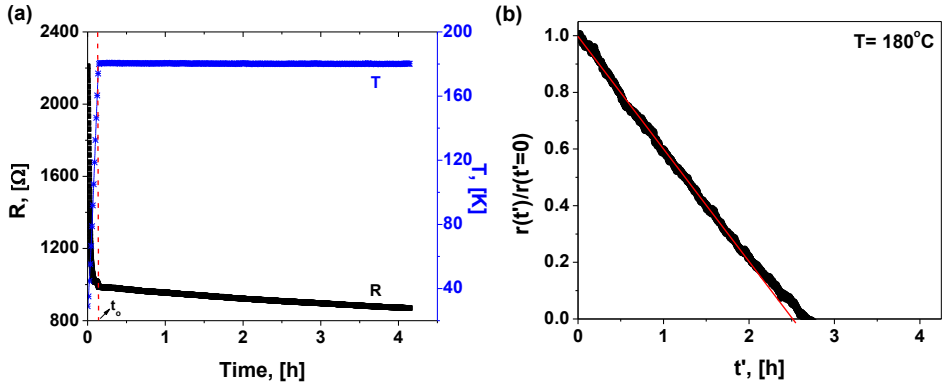

Fig. 4.11. (a) Resistance and temperature versus the heating time, due to the heating up effect point $t = 0$ was put to the t_o time belonging to the sharp kink on the temperature/time curve, (b) $r(t')/r(t' = 0)$ versus the corrected time t' at 180°C.

Now using the relations $k_1 = 1/R_1$, $k_2 = 1/R_2$ ($R_2 > R_1$, since the resistivity of NiSi is less than that of Ni_2Si) and $k = 1/R$, Eq. (4.4) can be rewritten as:

$$\rho^* = \left[\frac{\frac{R_1}{R}-1}{\frac{R_1}{R}+2}\right] A = r(t)\, A^* , \tag{4.5}$$

with $A^* = \frac{\left(\frac{R_1}{R_2}+2\right)}{\left(\frac{R_1}{R_2}-1\right)}$.

Thus, in principle the $r(t) = [\frac{R_1/R-1}{R_1/R+2}]$ function should be equal to $1/A^*$ at $t = 0$ ($R_1/R = R_1/R_2$) and equal to 0 at $t = \infty$ ($R_1/R = 1$).

What can one expect for the time dependence of ρ^*? At an intermediate t time the volume of the remaining Ni_2Si can be given as $4\pi(d/2)^3/3$, where d is the average diameter of the spherical particle not consumed yet. At $t = 0$, the radius is $d_o/2$ and $d = d_o - 2vt$, thus,

$$\rho^* = \frac{V_2}{V} = \left(\frac{d}{d_o}\right)^3 = \left(1 - \frac{2vt}{d_o}\right)^3 \cong 1 - \frac{6vt}{d_o} \tag{4.6}$$

if higher order terms of vt are neglected. Thus, it is expected that ρ^* will be a linear (decreasing) function at the beginning of the process.

If we take into account that the interface shift (with v velocity) starts after an incubation time (time to fill up the boundaries of δ width) then the above results should be corrected, because the kinetics of ρ^* will be described by (4.5) and (4.6) only after t_o. If we correct the time scale accordingly by introducing $t' = t - t_o$ then the $\rho^*(t')$ function at $t' = 0$ will be less than 1. Then, it is better to use the $\rho' = \rho^*(t')/\rho(t' = 0)$ normalized function. In this case, $\rho^*(t') = 1 - 6vt'/d_o - 3\delta/d_o$, and $\rho^*(t' = 0)$ can be estimated as $1 - 3\delta/d_o$ corresponding to the filled up boundary shells of δ width.

Thus,

$$\frac{r(t')}{r(t'=0)} = \frac{\left[\frac{R_1}{R(t')}-1\right]}{\left[\frac{R_1}{R(t')}+2\right]} \Big/ \frac{\left[\frac{R_1}{R(t'=0)}-1\right]}{\left[\frac{R_1}{R(t'=0)}+2\right]} = \frac{\rho^*(t')}{\rho^*(t'=0)} = 1 - t'\frac{\frac{6v}{d_o}}{\left(1-\frac{3\delta}{d_o}\right)} = 1 - mt'. \qquad (4.7)$$

Now, plotting of $r(t')/r(t' = 0)$ versus t' should yield a straight line at the beginning. For the construction of the above ratio we need the value of R_1. In principle, it should belong to $t' = \infty$ when the film has been fully transformed to NiSi. But according to Fig. 4.4 the process did not finish after reaching the NiSi phase, since there is a Si reservoir in contact with the film and this provides more and more additional Si atoms, resulting a gradual deviation from the stoichiometric composition of NiSi. Thus, it is not easy to find the value of R_1 from the resistance curve alone. But the value belonging to $c_{Si}/c_e = 1$ in Fig. 4.9 or the medial value of the time window at 180°C can be taken as the time when already the formation of the NiSi phase has been finished. The value of $R = 900\ \Omega$ belonging to this time ($t \cong 2.5h$) can be taken as R_1. Fig. 4.11(b) shows the $r(t')/r(t' = 0)$ versus t', constructed with the use of the above R_1 value. It can be seen that it is a good straight line (except the small deviations at around 0, which is probably the consequence of the approximation used). The origin of the t' scale (t_o) was taken at the point indicated by the vertical line in Fig. 4.11(a) (the first part of this curve reflects the effect of the fast increase of the temperature and

some relaxations in the structure). The velocity can be calculated from the initial slope of the straight line shown in Fig. 4.11(b), $m = 6v/(d_o - 3\delta)$, if d_o is known.

Taking $d_o = 7\ nm$, determined from the fitting of the straight line in Fig. 4.9, the velocity of the grain boundary diffusion induced interface motion is about 0.3×10^{-4} nm/s. This value is close to that obtained from the SNMS depth profiles and thus confirms our model.

4.2. Kinetics of shift of individual interfaces in Ni/Si system during low temperature reactions

Experimental results

Fig. 4.12 shows the concentration-depth profiles of the as-deposited and annealed samples of nanocrystalline-Ni/c-Si at 180°C for different annealing times. The position of the Ni/Si interface in the as-deposited sample was taken as zero point in the depth axis. It is clear that the solid state reactions between the nanocrystalline Ni film and the c-Si substrate led to the formation of product layer of Ni_xSi_{1-x} with $x \cong 0.5$. Furthermore, it can be seen that this product layer is not fully homogeneous and is Ni-rich at the Ni side. A closer look of curves at shorter times (at 0.25 and 1 h) reveals that the Ni rich composition is at about 60%, suggesting a formation of Ni_2Si layer first and with increasing annealing time the average composition in the reaction zone gradually approaches to the composition of the NiSi phase. Nevertheless the thickness of the overall product layer increases gradually with the annealing time by shifting its bordering interfaces in opposite directions i.e. consuming both the initial Ni and Si. It is important to emphasize that in the investigated time interval there is an *unlimited supply* of silicon and nickel, i.e. these result should be clearly distinguished from *supply limited* cases [101].

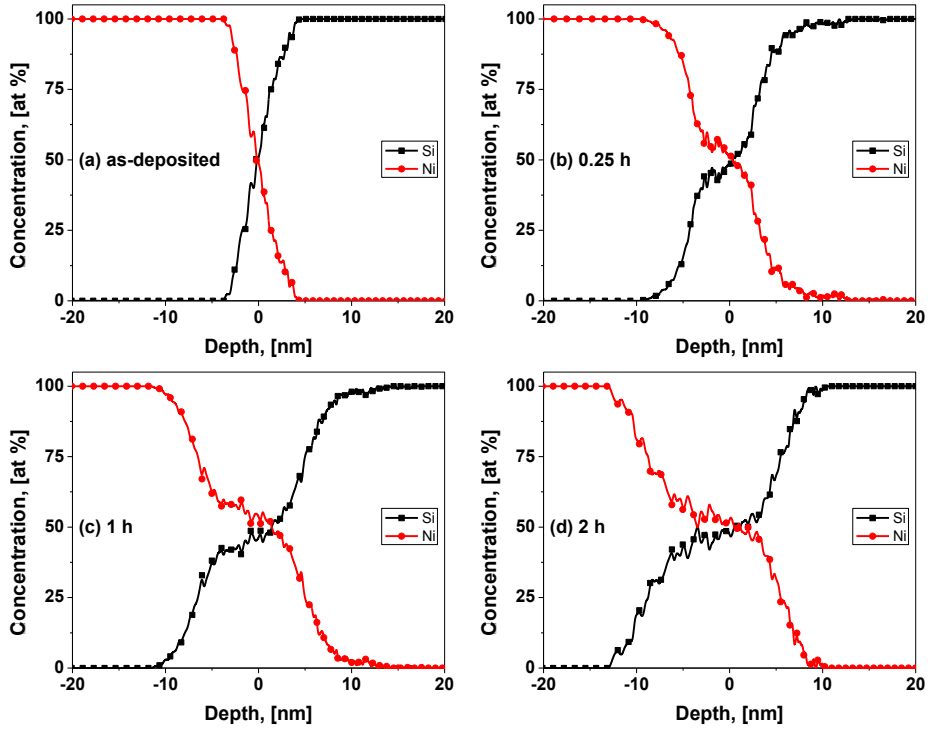

Fig. 4.12. Concentration-depth profiles of Ni(20nm)/c-Si: (a) as-deposited, (b)-(d) annealed at 180°C for different annealing times.

Fig. 4.13 shows the concentration-depth profiles for the as-deposited and annealed samples of nanocrystalline-Ni/amorphous-Si. It is clear that the product layers are wider than the corresponding ones in Fig. 4.12 (see e.g. the curves corresponding to $t = 2\ h$). Furthermore, again at short annealing time there is a shoulder on the Ni side with 0.6/0.4 Ni/Si ratio and additionally at longer times ($t \geq 1$ h) a new shoulder appears on the Si side suggesting also the formation of the $NiSi_2$ phase (see the arrow in Fig. 4.13(c)).

It is important noting that there are no visible penetrations of Si along Ni grain boundaries, since the Si profile in Ni is unchanged after heat treatments. This is in contrast to the observed remarkable Si penetration along Co grain boundaries [102] where even the formation of the reaction

layer with planar interfaces was not observed at 310°C between 1 and 24 hours annealing times.

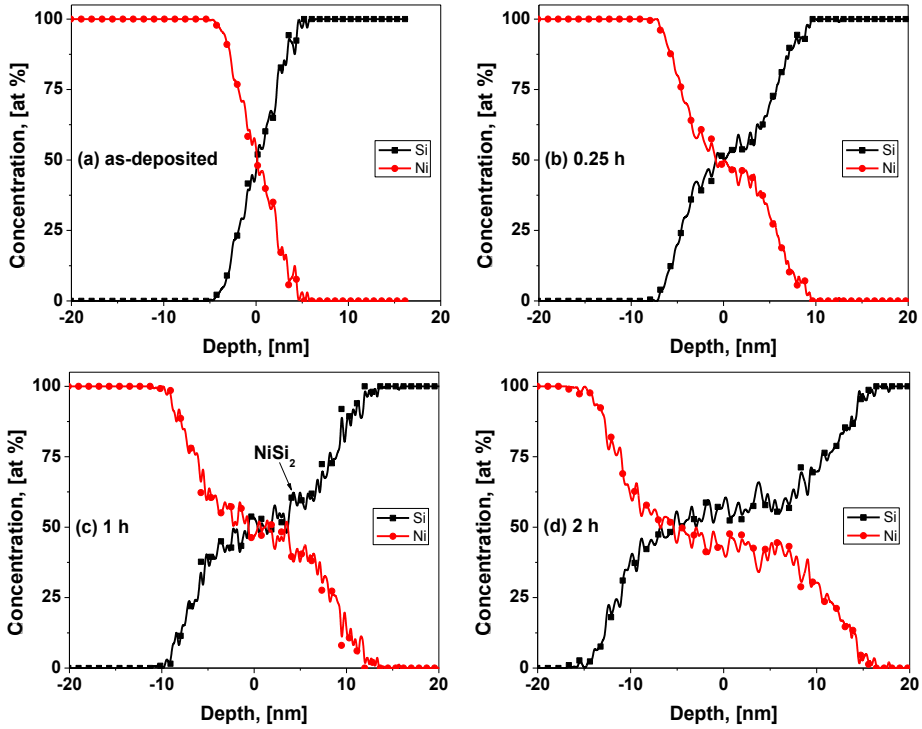

Fig. 4.13. Concentration-depth profiles of Ni(20nm)/a-Si(50 nm): (a) as-deposited, (b)-(d) annealed at 180°C for different annealing times (see also the text).

The XRD results (Fig. 4.14) show that in the annealed samples, there are peaks which can be attributed to Ni_2Si and/or NiSi in both types of samples.

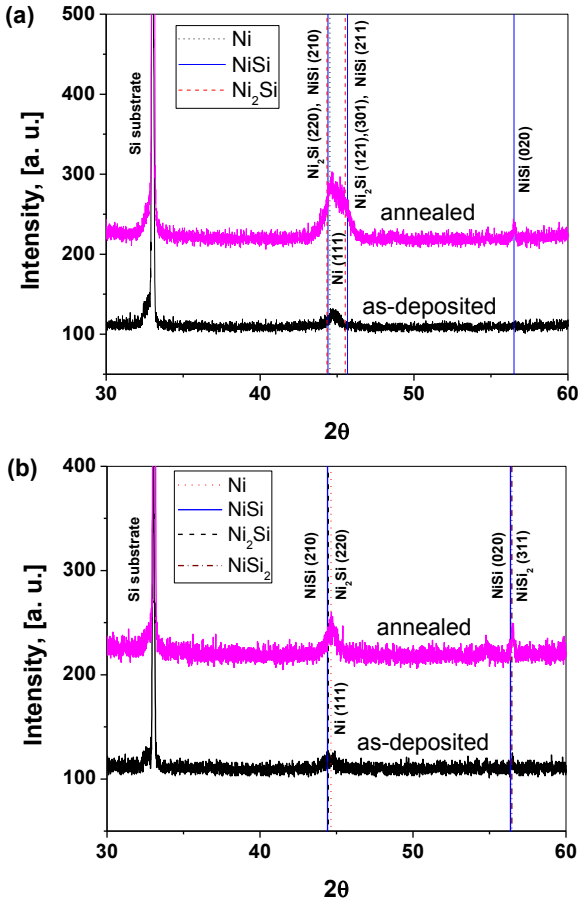

Fig. 4.14. XRD of the as-deposited and annealed samples at 180°C for 3h of: (a) Ni/c-Si and (b) Ni/a-Si.

In order to investigate the kinetics of the shift of interfaces bordering the reaction zone and that of the growth of the product layer, it is important to choose the position of the interfaces carefully. Since the position of the Ni/Si interface at concentration of 50% in the as-deposited sample was taken as zero point in the depth axis, the distance of the Ni/Ni_xSi_{1-x} and Ni_xSi_{1-x}/Si interfaces were measured from this zero point. The positions of the above interfaces were chosen at the points of inflection at about 75% as well as 25% Ni, respectively. Plots of the logarithms of (X), (Y) and $(X - Y)$ (up to 2h annealing time) versus log t show that the curves can be fitted by straight lines (Fig. 4.15(a)). The slopes of these lines are about 0.5. This means that these kinetics follow the parabolic growth law i.e. the change of the

thicknesses were proportional to $t^{1/2}$. To confirm this, the values of X, Y and $(X - Y)$ were plotted as functions of the time and the square root of time as shown in Figs. 4.15(b) and 4.15(c), and fitted assuming linear dependence. Comparison of the R^2 values of these fits confirms the parabolic growth law. Similar results were observed for Ni/a-Si as shown in Fig. 4.16 with the only difference that the shifts are larger here (the analysis of the linear/parabolic behavior resulted in the same conclusion, thus only the plots analogous to Fig. 4.15(c) are shown in Fig. 4.16). Note that the existence of the shoulders at the Ni side (in Ni/c-Si) and at both the Ni and Si sides (in Ni/a-Si) in Figs. 4.12 and 4.13 can make the determination of the position of the Ni_xSi_{1-x}/Si and Ni/Ni_xSi_{1-x} interfaces a bit uncertain if these are indeed indications of the appearance of different phases. As a first approximation we neglected this effect, i.e. our results for $(X - Y)$ versus time can be considered as the plot for the average growths of the reaction layer.

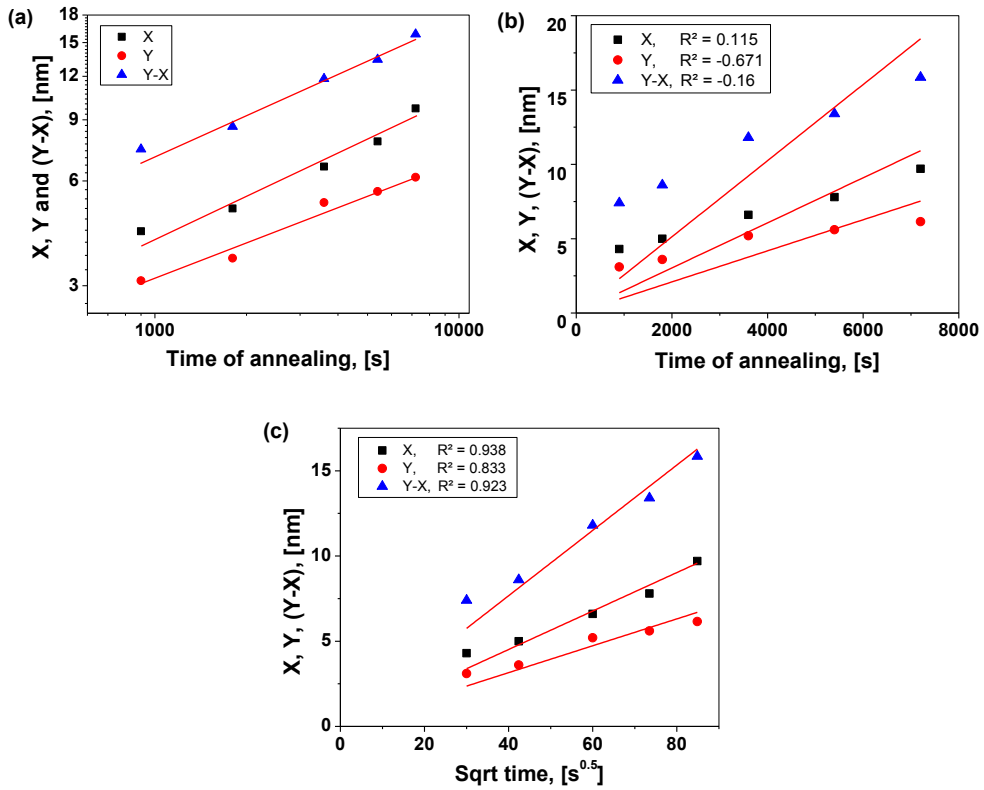

Fig. 4.15. Interface positions (X,Y) and phase thickness $(Y - X)$ as functions of the annealing time: (a) logarithmic scale, (b) linear scale, (c) square root of time scale for Ni(20nm)/c-Si.

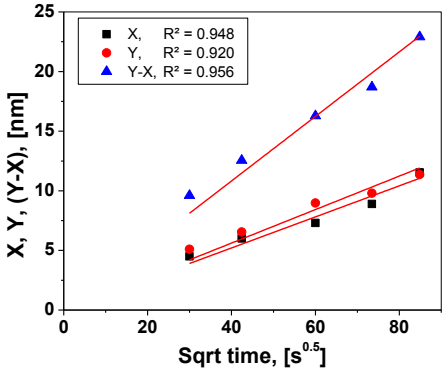

Fig. 4.16. Interface positions (X,Y) and phase thickness ($Y - X$) as functions of the square-root of annealing time for Ni(20nm)/a-Si(50 nm).

The effect of Pt on the solid state reactions is shown in Fig. 4.17 and 4.18. For Ni/c-Si (Fig. 4.17), the Pt – in accordance with the literature [70-72] - enhances the homogeneity of the product layer with a composition of the NiSi phase and the NiSi/Si and Ni/NiSi-interfaces are sharper.

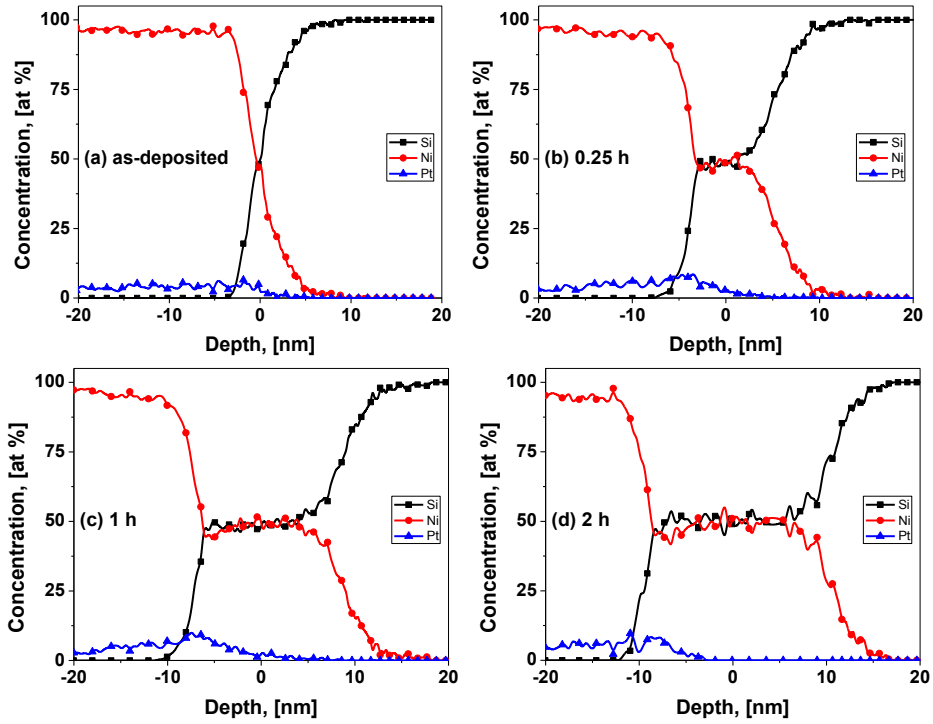

Fig. 4.17. Concentration-depth profiles of Ni(5%Pt)(20nm)/c-Si: (a) as-deposited, (b)-(d) annealed at 180°C for different annealing times.

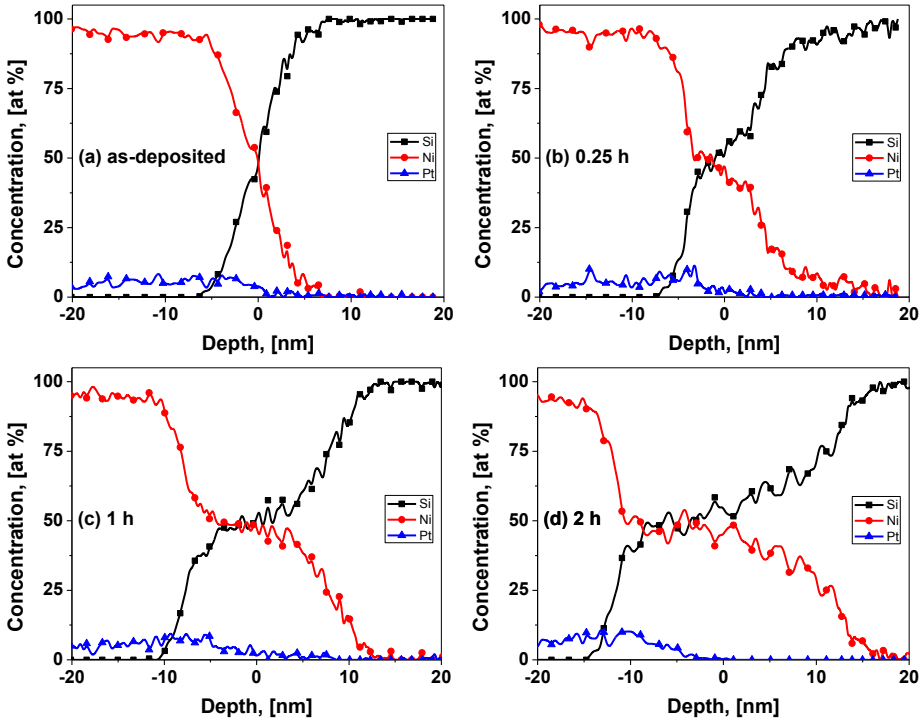

Fig. 4.18. Concentration-depth profiles of Ni(5%Pt)(20nm)/a-Si(50 nm): (a) as-deposited, (b)-(d) annealed at 180°C for different annealing times.

For Ni/a-Si (Fig. 4.18), the Pt again enhances both the homogeneity of the product layer (with a composition corresponding to NiSi) and the sharpness of the interface on the Ni side. At the same time on the Si side the product layer still has a shoulder at the composition of about $NiSi_2$.

Fig. 4.19 shows the XRD results of the as-deposited and the annealed samples for Ni(Pt)/c-Si and Ni(Pt)/a-Si. It is clear that, similarly to Fig. 4.14, there are peaks in the annealed samples which can be related to Ni_2Si and NiSi in Ni(5%Pt)/c-Si and to Ni_2Si, NiSi and $NiSi_2$ in Ni(5%Pt)/a-Si.

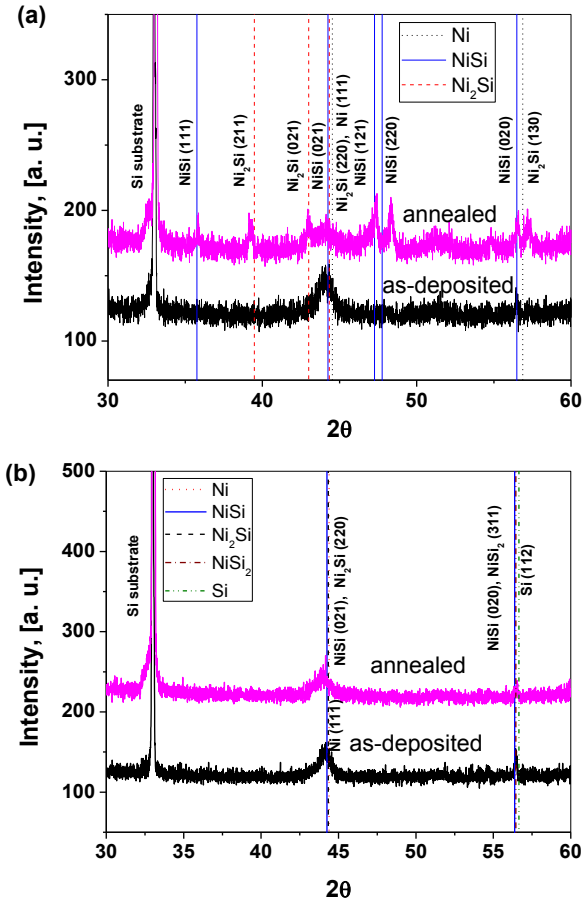

Fig. 4.19. XRD of the as-deposited and annealed samples at 180°C for 3h: (a)Ni(5%Pt)/c-Si (b) Ni(5%Pt)/a-Si.

Similar plots can be created for the shift of the interfaces and the growth of the product phase like those shown in Figs. 4.15 and 4.16. From the analysis of the fits it was again concluded that they obey the parabolic law as shown in Fig. 4.20 (a, b). Although 5% of Pt has strong influence on the homogeneity of the product layer and sharpening of the interfaces, it has no effect on the growth kinetics.

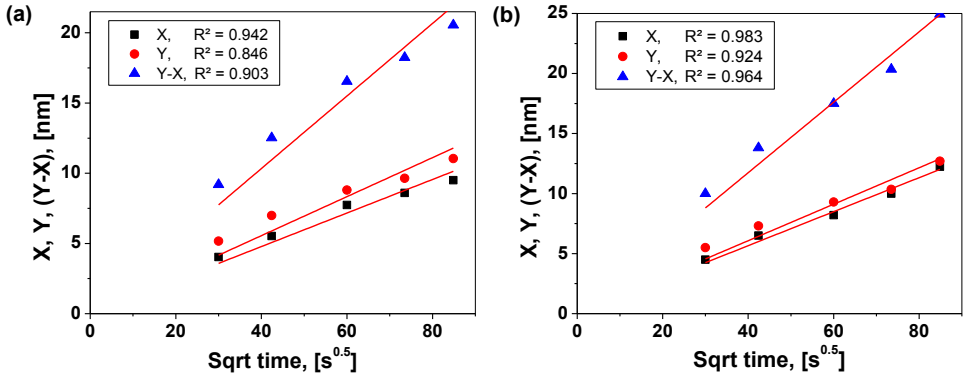

Fig. 4.20. Interface positions (X,Y) and phase thickness ($Y - X$) as functions of the square-root of annealing time for: (a) Ni(5%Pt)/c-Si, (b) Ni(5%Pt)/a-Si.

Discussion and conclusions

a) Ni/a-Si system

As one can see from Fig. 4.13(a), the Ni/a-Si interface is a bit wider than that of for the Ni/c-Si system (see Fig. 4.12(a)) in as-deposited state, but our depth resolution limits us from getting an unequivocal conclusion about the presence of an amorphous silicide layer in the Ni/a-Si system, as observed in [60] and [61]. It is worth noting that as a consequence of the formation mechanism of such an initial layer (dynamic segregation effect: the lower surface energy of Si helps the intermixing when the Ni is deposited on it) it is expected that the appearance of the amorphous silicide layer also depends on the conditions of the film deposition (e.g. substrate temperature, sputtering rate).

At short annealing times there is a small shoulder at the composition of Ni_2Si and the reaction zone is not homogeneous, containing a gradient (the composition changes between 60% and 40% of Ni). This is in accordance with Refs. [60,62,63], where it was observed that regions with two different compositions, corresponding to Ni_2Si and NiSi, formed. Although from our results we cannot decide whether the Ni_2Si phase develops (between Ni and the amorphous/crystalline NiSi) with a planar growth mode or not, we can conclude that *the Ni shrinkage follows a*

parabolic law i.e. it is diffusion controlled. This can be an important contribution to the apparently controversial literature results on a possible planar or non–planar growth of crystalline Ni_2Si (and the corresponding parabolic [63] or linear growth in the first stage [65]): at least the Ni consumption is parabolic. It is worth noting that in [65] the growth of the crystalline Ni_2Si phase was followed by such methods (DSC, XRD) which do not provide information about the morphology of the growing phase. Thus, their results rather characterize the overall increase of the amount of the Ni_2Si phase but whether this phase had a planar interface with NiSi region or not could not be decided from the above type of measurements only.

At longer annealing times (longer than 1 h), Fig. 4.13(c) illustrates that a plateau develops at compositions of about 40% Ni on the a-Si side suggesting the formation of the $NiSi_2$ phase. Comparison of Fig. 4.13(d) with Fig. 4.12(d) also reveals that this growths at the expense of amorphous Si. This can be related to the fact that the Ni diffusion coefficients in amorphous Si can be comparable with the GB diffusion coefficients in the growing silicides. It was published in [103] that elements like Cu and Pd have very low solubility in amorphous Si and they are fast diffusers. Although it was mentioned in [103], that the authors were not able to measure the diffusivity of Co, Ni and Fe, because of the very low solubility of these elements, it was predicted that these should also be fast diffusers in a-Si. Thus, according to Fig. 4.13 of [103] the diffusivity of the Ni should be even higher than that of Cu at 177°C: $1x10^{-17}m^2/s$. Furthermore, according to [62], the grain boundary diffusivity of Ni in Ni_2Si is about 5 orders of magnitude less than the above value. Taking into account that on the Si side the amorphous NiSi can be formed, in which a similar diffusivity is expected as for the Ni diffusion in a-Si, the intensive intermixing between a-NiSi and a-Si and the enhanced shrinkage of the a-Si is understandable. On the other hand, the Ni diffusion in single crystalline Si at 177°C is about $5.8x10^{-32}$ m^2/s, which explains why there is no $NiSi_2$ formation at the c-Si interface: the Ni penetration into the Si bulk is fully negligible and the Si shrinks just only because of the Si dissolution into the reaction zone.

In addition our results show *that the Si shrinkage is also diffusion controlled, i.e. follows the parabolic growth law*.

b) Ni/c-Si system

Our results shown in Fig. 4.12 are also in accordance with the literature results summarized in Chapter 2. The presence of the Ni_2Si phase can be identified and at the same time there is relatively large composition gradient present, similarly to the results of Refs. [66,67]. Note that here no traces for the formation of the $NiSi_2$ phase are detected. This is plausible if we take into account the above explanation about the diffusivities.

Both measured interfaces shift by parabolic law, and the shrinkage of Si is fully due to the dissolution of Si into the growing reaction layer.

c) Effect of Pt addition

The results shown in Figs. 4.17 and 4.18 clearly indicate the stabilization effect of Pt: in both (a-Si and c-Si) cases practically only a wide homogeneous region with NiSi composition can be observed. Thus, from our results, we conclude that only the NiSi phase formed and grew with parabolic mode. We cannot make a statement about the presence of Ni_2Si seeds: if they are present their amount should be small enough to result in measurable change in the composition within the limit of our method. The only difference between the plots obtained with a-Si and c-Si is that at longer annealing times, similarly to the case without Pt, the $NiSi_2$ appears on the Si side with a-Si layer. The same arguments as used above can be repeated here for the interpretation of this observation.

Finally, Fig. 4.21 shows the comparison of the Ni and Si shrinkages versus the annealing time at 180°C for all the investigated cases. It can be seen that both the Ni and Si shrinkage are a bit faster for a-Si than for c-Si in both samples with and without Pt addition. Especially the difference between the Si shrinkage in Ni/a-Si and Ni/c-Si is considerable (Fig. 4.21(b)). This can be related to the above mentioned fact that in the Si shrinkage not only Si-consumption during Si GB diffusion into the reaction layer is important but the a-Si shrinks also because of the Ni penetration into it.

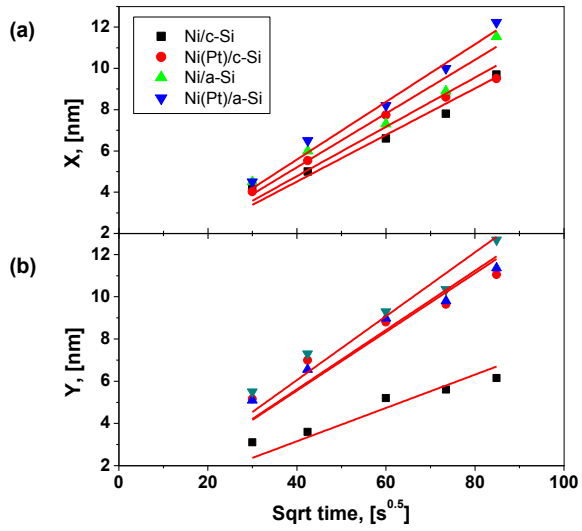

Fig. 4.21. Shrinkage of Ni (a) and Si (b) versus the annealing time at 180°C.

4.3. Grain boundary intermixing in Ag/Au thin film system and nanoscale Kirkendall porosity formation.

Fig. 4.22 shows the concentration-depth profile of the as-deposited Ag(15nm)/Au(15nm) bilayer. Fig. 4.23 (a-d) shows the concentration-depth profiles at different annealing temperatures (120, 150, 170, 200°C, respectively) for different annealing times under low (1 bar) pressure. It can be seen that there is an intensive intermixing and the average compositions in the centre of Ag and Au after 20 hours reached levels of 14-31% of Au and 19-37% of Ag, respectively, as shown in Fig. 4.24(a-d). These are definitely higher than the value due to any possible atoms concentrated in the cores of the GBs only. It should be about $c = 7.5\,\%$ as estimated assuming $\delta = 0.5\,nm$ for the grain boundary width and taking d_o about 20 nm (see the TEM picture below): $c \cong 3\delta/d_o$. It is worth mentioning that there is no planar diffusion zone at around the original interface, which would be expected e.g. in case of a pure bulk diffusion intermixing. It is clear that these saturation values increase with increasing the annealing temperature but still less than 50%.

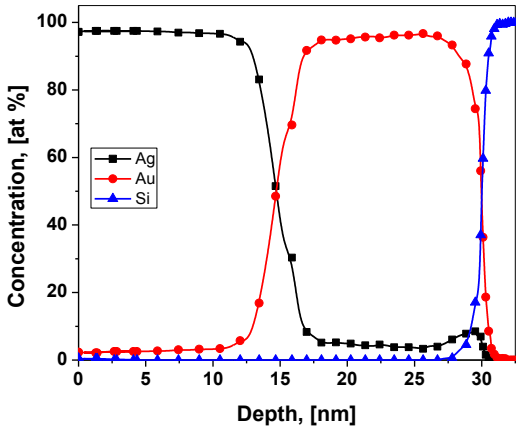

Fig. 4.22. Concentration-depth profile of as-deposited Ag(15nm)/Au(15nm) bilayer.

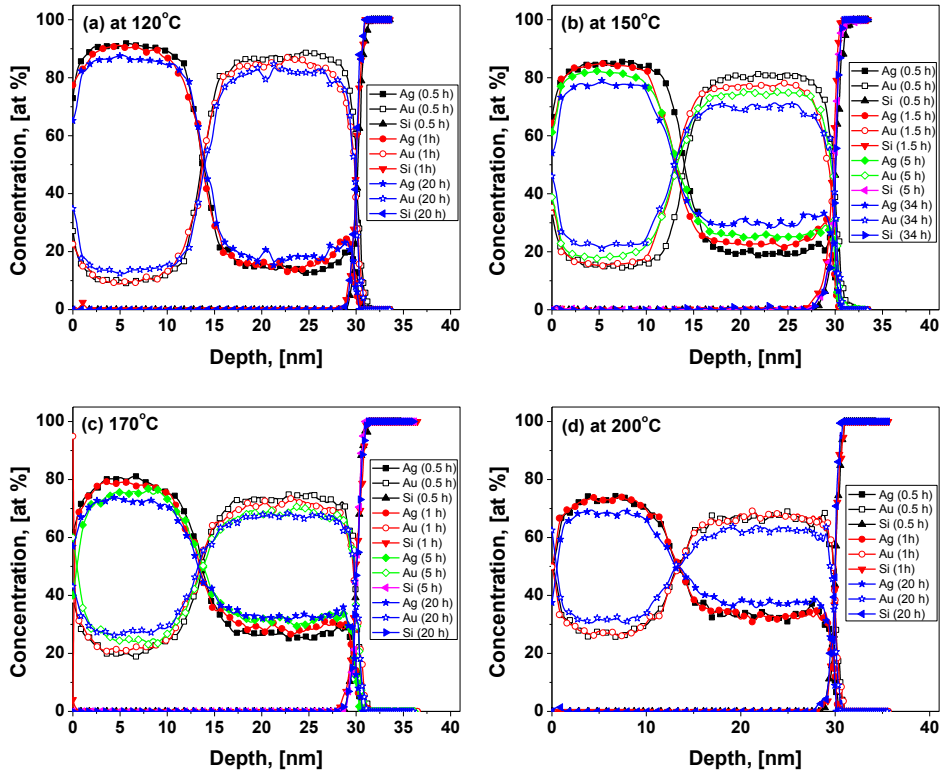

Fig. 4.23(a-d). Concentration-depth profile of Ag(15nm)/Au(15nm) bilayer annealed at 120-200°C, respectively, under low (1 bar) pressure.

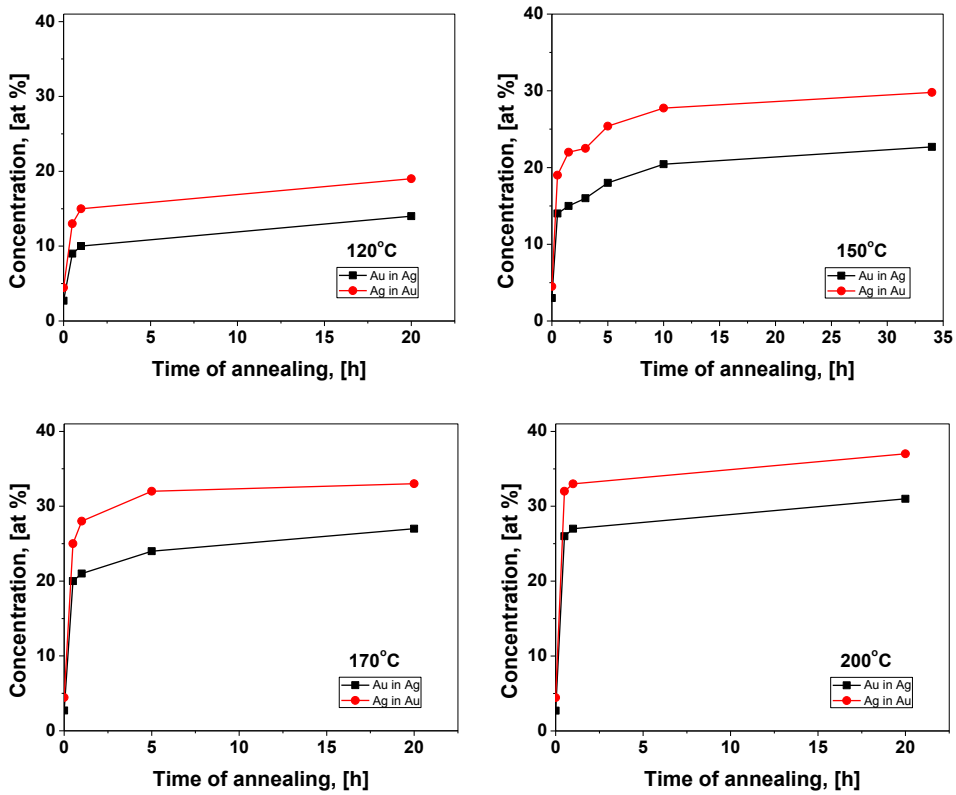

Fig. 4.24(a-d). Average concentration of Au and Ag inside the Ag and Au layers versus the annealing time at different annealing temperatures (120-200^{o}C, respectively) under low (1 bar) pressure.

For further investigation, the samples have been annealed under low (1 bar) and high (100 bar) pressures at 150^{o}C for 5h. The concentration-depth profiles of these samples are shown in Fig. 4.25. It can also be seen that the composition profiles are the same, within experimental errors, at the two different pressures. The TEM pictures of these samples are shown in Fig. 4.26(a and b). In Fig. 4.26(a), there are nanopores at the Ag grain boundaries and especially at triple junctions (see the arrows in Fig. 4.26(a)). On the other hand, there are no pores present in Fig. 4.26(b). The average grain size was estimated to be about 20 nm.

While there are nanopores at the GBs and triple junctions of Ag in samples annealed at 1 bar, there is no porosity in samples heat treated under

100 bar pressure (Fig. 4.26 a and b). This is what one would expect from the analogy of the effect observed in bulk Cu/Ni interdiffusion couple [13,78]. It was also shown in [13] that the porosity formation and the Kirkendall shift competed with each other: the shift was considerably larger when the pore formation was suppressed. Accordingly, since the DIGM can be considered as a special way of relaxation of stresses created by the inequality of GB fluxes, a similar competition would be expected between the GB porosity formation and DIGM: the latter should be faster under high pressure. Note that in [104] it was observed that the DIGM was a bit stronger in the film with low constraint case (free standing film) as compared to the high constraint case (film on the substrate).

We were not able to show changes in DIGM by the application of different pressures: the composition profiles at high and low pressures were the same within the experimental errors.

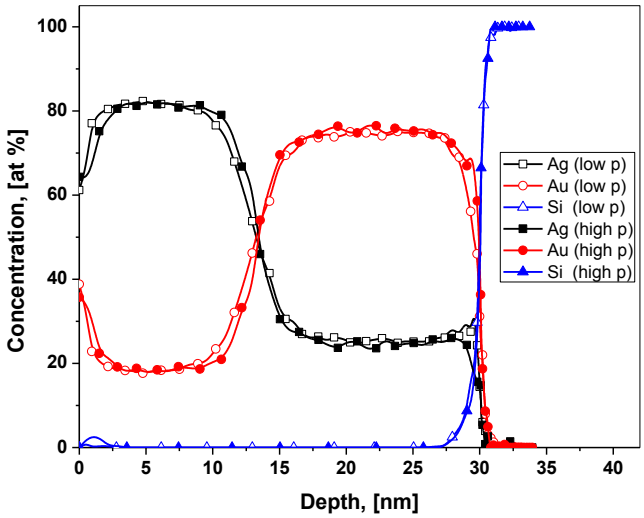

Fig. 4.25. Concentration-depth profile in Ag(15nm)/Au(15nm) bilayer annealed at 150^{o}C for 5h under low (1 bar) and high (100 bar) pressure.

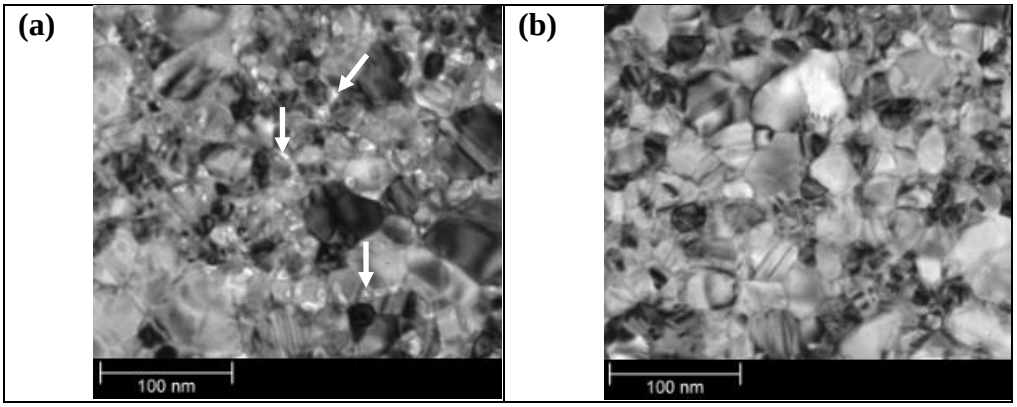

Fig. 4.26. Top view TEM of Ag(15 nm)/Au(15nm) bilayer annealed at 150°C for 5 h under (a) low (1 bar) and (b) high (100 bar) pressure.

Experimental results showed that in this system measurable DIGM occurred in Au even at low temperatures (at 150-200°C [104] as well as at room temperature [105]). In addition, using Auger depth profiling, similar composition versus depth profile was obtained at 250°C in [104] like shown in our Fig. 4.23(a-d). The increase of the composition in the plateau was interpreted by the formation of Ag alloyed zone by DIGM of Au GBs. The differences between their and our investigations, besides the application of 100 bar pressure, were that the grain size of the film was about 330 nm in [104] and that they did not investigate the processes in the Ag layer. The authors, using the linear relation between the average migration distance of the boundaries, L, and the average composition in the plateau region, c_{av}, plotted L versus the annealing time, t, at 250°C and showed that the migration rate decreased with increasing t and saturated at about 55 nm shift (see Fig. 13 in [104]). At the same time, the composition left behind the moving boundary, $c_b \cong 20\%$, was estimated from scanning transmission electron microscopic (STEM) investigation in the sample annealed at 200°C. Since the grain size in [104] was larger than two times of the above distance, the slowing down of the increase of the L was caused by slowing down the migration rate.

It can be seen from Fig. 4.24(a-d) that we also got saturation type time dependence with about c_{sat} equals 14-31% Au and 19-37% Ag saturation

values in the Ag and Au layers, respectively. However, in our case this saturation should be caused by the gradual overlapping of DIGM regions, resulting in the consumption of the original pure Ag and Au grains, since our grain size is about 5 times less than double of the estimated migration distance ($2\,L$). Thus, our c_{sat} values belong to the composition left behind the moving boundaries. In fact values of c_{sat} in Au are not too far from the value c_b estimated in [104].

The overall intermixing takes place on both sides of the diffusion zone (Fig. 4.23). Although, there are several publications in the literature on DIGM in the *faster* diffusing components (see e.g. [76] for DIGM in Cu of the Ni/Cu pair, [106] for DIGM in Cr of the Cr/W system), in the majority of cases the DIGM was investigated on the side of the *lower* component in which $J_A > J_B$ (in our case in the Au layer, where $J_{Ag} > J_{Au}$). Our results demonstrate that if the grain size is small enough (less than two times the migration distance before the DIGM slows down considerably) a homogenization in a bilayer film is possible on *both* sides. The saturation values are visibly different in Ag and in Au. It is an interesting question: whether a full homogenization is possible exclusively by DIGM or not? The composition gradient is still present in our samples after reaching the saturation: are there any kinetic passes to proceed further after the saturation levels which are less than 50%? The understanding of the above questions is important for many technological aspects of nanomaterials: for instance effective low temperature homogenization can be reached by DIGM in systems, where intermetallic compounds can be formed (see e.g. [19]).

As a first assumption, one can assume that these saturation levels may be due to miscibility gap in the phase diagram. This assumption cannot be accepted since the heat of mixing is negative in Ag/Au system. So, these saturation levels can not correspond to equilibrium values. In this case what is the reason behind of such saturation? In order to understand this, we prepared samples with approximately the same initial compositions as the saturated sample at 170^{o}C. The concentration-depth profile of this Ag(27%Au)/Au(31%Ag) as-deposited sample is shown in Fig. 4.27. The sample was annealed at 170^{o}C for different times and the concentration-depth profiles are shown in Fig. 4.28. It is clear that there is still intermixing on both sides reaching higher saturation levels (see Fig. 4.29). This confirms

that the saturation levels of the initially pure Ag/Au samples do not correspond to equilibrium values. These initial saturation levels are the results of some kind of kinetic constrain. These constrains can be related to two possible reasons:

1) They have been developed by stress fields caused by the initial inequality of the GB fluxes. After reaching certain saturation, they do not allow further DIGM, since they compensate the difference of the two fluxes (see the expression for the flux in Eq. (1.35) which contains a term proportional to the stress gradient).

2) They are due to finite size effect: for thin films, the composition gradient along the GBs should gradually decrease (because of the reflections from the film boundaries) and thus the interface velocity can also gradually decay, since it is proportional to the second derivative of the composition (see Eq. (1.38))

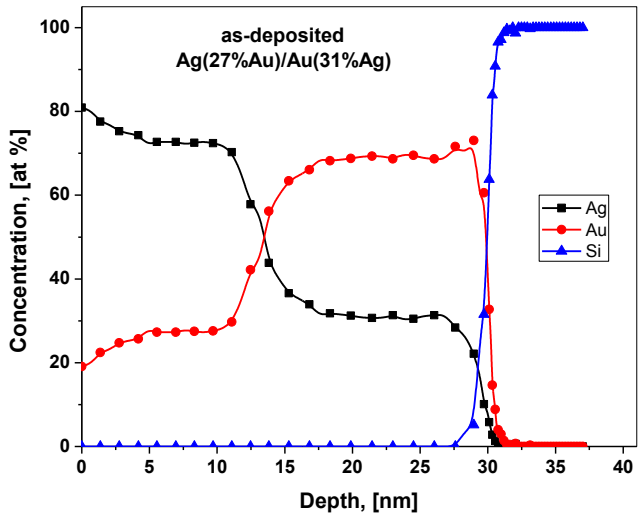

Fig. 4.27. Concentration-depth profile of as-deposited Ag(27%Au)/Au(31%Ag) bilayer.

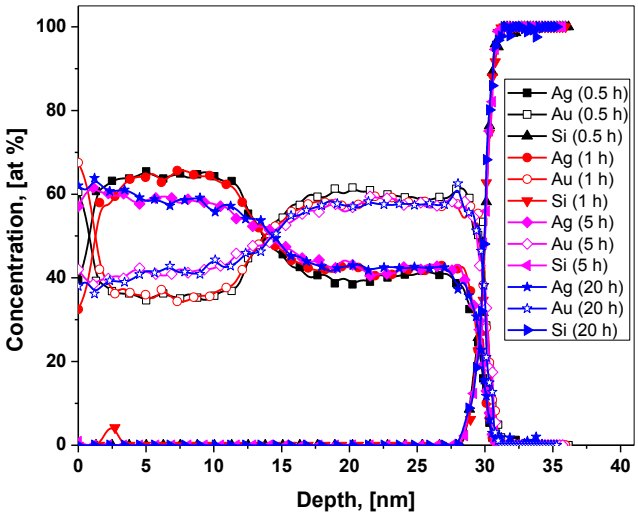

Fig. 4.28. Concentration-depth profile of Ag(27%Au)/Au(31%Ag) bilayer annealed at 170°C for different annealing times.

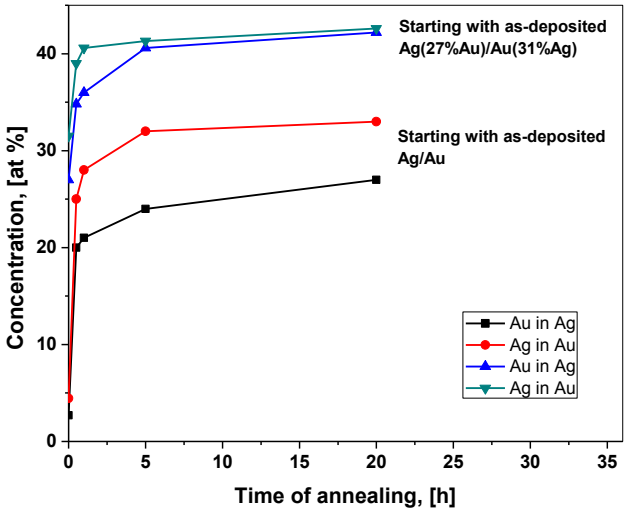

Fig. 4.29. Average concentration of Au and Ag inside the Ag and Au layers versus annealing time at 170°C in initially Ag/Au and Ag(27%Au)/Au(31%Ag) bilayers.

Conclusions

1. Ni_2Si/c-Si system

1.1. Solid state reaction between the nanocrystalline Ni_2Si and c-Si substrate led to subsequent NiSi and $NiSi_2$ reaction layer formation depending on the temperature, time and film thickness. There exist certain temperature-time and thickness-time windows for the formation of technologically important NiSi.

1.2. NiSi is formed by grain boundary diffusion induced solid state reaction (GBDIREAC); i.e. by formation of the NiSi phase at the grain boundaries and by growing perpendicular to the grain boundary plane consuming the parent grains.

2. Ni/Si systems

2.1. Solid state reactions in Ni/Si systems, with both amorphous and single crystalline Si (100) substrate, at low temperature lead to formation of a product layer (Ni_2Si + NiSi) with *relatively large composition* gradient in it.

2.2. Our method allowed determination of the kinetics of shift of individual interfaces (i.e. the Si and Ni shrinkage) as well as the average growth kinetics of the product layer in the very early stage of the solid state reaction. They followed *the parabolic growth law in both systems* i.e. controlled by diffusion only.

2.3. In a-Si the $NiSi_2$ is formed at long annealing times on the Si side due to the high diffusivity of Ni in a-Si.

2.4. Presence of 5%Pt enhances the homogeneity of the product layer and the sharpening of the interfaces, but do not influence the growth kinetics.

3. Ag/Au system

3.1. We have provided clear experimental evidence on the formation of nano pores in GBs of Ag in Ag/Au nanocrystalline thin films at low temperature where the bulk diffusion is completely frozen out.

3.2. In analogy with bulk interdiffusion the formation of this porosity can be suppressed by application of about 100 bar hydrostatic pressure.

3.3. We demonstrated that the homogenization is possible by DIGM in both Ag and Au films, at least up to the level corresponding to the compositions left behind the moving boundaries.

3.4. The saturation levels, less than 50%, do not correspond to equilibrium values. They are the result of some kind of kinetic constrains which are due to the development of a stress gradient, compensating the difference of the two grain boundary fluxes. These constrains could be also due to the finite size effect, decaying the interface velocity.

Summary

This thesis is about the investigation of diffusion and solid state reactions in thin film systems in the nanoscale at relatively low temperatures (120-200^{o}C). The systems are nanocrystalline-Ni_2Si/crystalline-Si, nanocrystalline-Ni/c-Si, Ni(Pt)/c-Si, Ni/amorphous-Si, Ni(Pt)/a-Si and Ag/Au. I prepared these systems by DC magnetron sputtering. Then, I annealed the samples in high vacuum furnace except the Ag/Au system which was annealed under low and high hydrostatic pressure (in argon of 99.999% purity). After that I investigated the samples using secondary neutral mass spectrometry. It provides intensity-sputtering time profiles. These profiles were converted to concentration-depth profiles by knowing the sensitivity factors of the elements and measuring the depth of the sputtered craters at different depths by profilometer.

In the first part of my thesis, I studied the solid state reaction between Ni_2Si and Si(100) substrate at low temperatures (180-200^{o}C). The solid state reaction led to subsequent NiSi and $NiSi_2$ reaction layer formation depending on the temperature, time and film thickness. There exist certain temperature-time and thickness-time windows inside of which the formation of NiSi takes place. The technologically important NiSi is formed by grain boundary diffusion induced solid state reaction (GBDIREAC), i.e. the NiSi phase is formed at the grain boundaries and grown by the motion of these boundaries perpendicular to the grain boundary plane consuming the parent Ni_2Si grains. These results were confirmed by XRD and TEM measurements. The velocity of the grain boundary diffusion induced interface motion was estimated from the depth profiles of the first stage of the process using the linear dependence

of the average composition inside the film on the annealing time. The normalized value of the resistance, proportional to the amount of the new phase, showed also similar time evolution and yielded similar value for the interface velocity. [papers 1, 4 and 5]

In the second part of my thesis, I studied the kinetics of shift of individual interfaces in Ni/c-Si and Ni/a-Si systems as well as the average growth kinetics of the product layer in the very early stage of the solid state reaction (at 180^{o}C for 0.25-2 h). The solid state reactions in both systems lead to formation of a product layer (Ni_2Si + NiSi) with relatively large composition gradient in it. The kinetics of the Si and Ni shrinkage followed the parabolic growth law in both systems i.e. the change of the thicknesses was proportional to square root of the annealing time. In systems with a-Si, at longer annealing times, a layer with composition of about 40% Ni was developed suggesting the formation of the $NiSi_2$. This was interpreted by the relatively high diffusivity of Ni in a-Si. Presence of 5%Pt enhances the homogeneity of the product layer and the sharpening of the interfaces, but do not influence the growth kinetics. [paper 2]

In the third part of my thesis, I studied the grain boundary intermixing in Ag/Au thin film system at low temperatures (120-200^{o}C) for different times, where the bulk diffusion processes are completely frozen out. Clear experimental evidence is provided on nanoscale Kirkendall porosity formation along grain boundaries in Ag during the intermixing. Application of 100 bar pressure suppressed the porosity formation. The interdiffusion leads to homogenization in both the Ag and Au layers up to levels corresponding to compositions left behind the moving boundaries during grain boundary diffusion induced grain boundary motion (DIGM). The homogenization corresponds to saturation levels, less than 50%, which would be expected for a system with complete mutual solubility, like Ag/Au. These levels resulted from kinetic constrains, due to the development of a stress gradient, compensating the difference of the two grain boundary fluxes. Also, these constrains could be due to the finite size effect, decaying the interface velocity, by reducing the second derivative of the GB composition. [paper 3]

All the results summarized in this thesis are my own achievements.

Summary in Hungarian (Összefoglalás)

Ez a tézisfüzet vékony rétegekben alacsony hőmérsékleteken (120-200^{o}C) lejátszódó, szemcsehatár diffúzió kontrollált keveredésre és szilárdtest reakciókra vonatkozó eredményeket tartalmaz nanokristályos-Ni_2Si/kristályos(c)-Si, nanokristályos-Ni/c-Si, Ni(Pt)/c-Si, Ni/amorf(a)-Si, Ni(Pt)/a-Si és Ag/Au vékonyrétegekben, melyeket magnetronos porlasztással készítettem. A mintákat vákuum kemencében hőkezeltem az Ag/Au rendszer kivételével, amelyet kis és nagy hidrosztatikai nyomáson hőkezeltem (99.999% tisztaságú argonban). A próbatesteket másodlagos semleges tömeg-spektrométerrel, (Secondary Neutral Mass Spectrometry) vizsgáltam, amely intenzitás-porlasztási idő profilokat szolgáltat. Ezeket, az elemek érzékenységi faktorainak ismeretében és a porlasztott kráterek mélységét profilométerrel meghatározva, összetétel-mélység függvényekké alakítottam át.

Téziseim első részében Ni_2Si és Si(100) hordozó közötti szilárdtest reakciót vizsgáltam alacsony hőmérsékleteken (180-200^{o}C). A reakció, egymást követően, NiSi és $NiSi_2$ reakció rétegek képződéséhez vezetett és a részletek függtek a hőmérséklettől, az időtől és a kiindulási rétegvastagságtól. Megmutattam, hogy léteznek bizonyos hőmérséklet-idő illetve vastagság-idő ablakok, amelyen belül a NiSi fázis képződése játszódik le. A technológiailag fontos NiSi keletkezése szemcsehatár diffúzió által indukált szilárdtest reakcióval (GBDIREAC) játszódik le, azaz a NiSi fázis a szemcsehatárokon képződött és a fázishatároknak erre merőleges mozgásával nőtt, elfogyasztva a Ni_2Si szemcsék anyagát. Ezeket az eredményeket XRD és TEM vizsgálatokkal is megerősítettem. A szemcsehatár diffúzió indukálta határfelület mozgás sebességét a koncentrációnak a film belsejében az idő függvényében történő növekedéséből, amely a folyamat első szakaszán lineárisnak adódott, becsültem meg. A normált elektromos ellenállás, amely szintén arányos az új fázis

mennyiségével, hasonló időfüggést mutatott és hasonló értéket adott a határfelület eltolódási sebességére.

Téziseim második részében a fázisokat elválasztó határfelületek eltolódási kinetikáját vizsgáltam Ni/c-Si és Ni/a-Si rendszerekben valamint a keletkezett réteg átlagos növekedési kinetikáját határoztam meg a szilárdtest reakció legelső szakszán (180^{o}C-on 0.25-2 órás kezeléseknél). Mindkét rendszerben a szilárdtest reakció egy (Ni_2Si + NiSi) reakció-réteg keletkezéséhez vezetett, amelynek belsejében jelentős összetétel gradiens volt jelen. A Si és a Ni fogyása parabolikus törvényt követett mindkét rendszerben, azaz a vastagság az idő négyzetgyökével arányosan nőtt. Az a-Si-ot tartalmazó rendszerben, hosszabb időknél, egy kb. 40%-os Ni tartalmú réteg is kifejlődött $NiSi_2$ fázis képződést is sugallva. Ezt a Ni-nek az amorf Si-ban való viszonylag gyors diffúziójával magyaráztam. 5% Pt jelenléte elősegíti a képződött réteg homogenitását és az eltolódó határfelületek élességét, de nincs befolyással a kinetikára.

A harmadik részben szemcsehatár diffúziós keveredést vizsgáltam Ag/Au vékony filmekben alacsony hőmérsékleteken (120-200^{o}C) ahol a térfogati diffúzió teljesen befagyott. Egyértelmű kísérleti bizonyítékot szolgáltattam Kirkendall nano-porozitások keletkezésére az Ag szemcsehatárokon. 100 bar hidrosztatikai nyomás megszüntette a pórusképződést. A kölcsönös diffúzió mind a két (Ag és Au) rétegben homogenizációt eredményezett olyan koncentrációkig, amely megfelelt a diffúzió indukált szemcsehatár mozgással (DIGM) mozgó határok által maguk mögött hagyott tartomány koncentrációjának. Az ennek megfelelő telítési koncentrációk 50%-nál kisebbek, bár ez lenne várható egy ideális rendszer, (mint amilyen az Ag/Au rendszer is) teljes keveredésekor. Ezeket a telítési értékeket kinetikus kényszerek eredményezhetik, amelyeket a két szemcsehatár áram különbségéből felépülő feszültségek eredményezhetnek, illetve véges-méret hatások (idővel csökken a szemcsehatárban a koncentráció második deriváltja) is szerepet játszhatnak.

Az ebben a tézisfüzetben ismertetett eredmények az én saját eredményeim.

References

[1] Bence Parditka, Investigation of diffusion and solid state reactions on the nanoscale in Silicon based systems of high industrial potential: experiments and simulations, PhD thesis, 2014.

[2] J. Philibert, Atom movements - Diffusion and mass transport in solids, Les Ulis, France, Les Editons des Physique, 1991.

[3] A.R. Allnatt and A.B. Lidiard, Atomic Transport in Solids, Cambridge: University Press, 1993.

[4] D.L. Beke, General Introduction in "Diffusion in Semiconductors and Non-Metallic Solids" Landolt-Börnstein New Series III/33A (ed. D.L. Beke) Springer, Berlin, 1998.

[5] C.P. Flynn, Point Defects and Diffusion, Oxford, Clarendon Press, 1972.

[6] J.R. Manning, Diffusion Kinetics of Atoms in Crystals, Princeton: van Nostrand, 1968.

[7] Ya.E. Geguzin and M.A. Krivoglaz, Migration of Macroscopic Inclusions in Solids, New York, Consultans Bureau (Plenum Publ.), 1973.

[8] D.L. Beke, Defect Diffus. Forum **129-130** (1996) 9.

[9] L.S. Darken, Trans. Am. Inst. Min. Metall. Eng. **175** (1948) 184.

[10] D.L. Beke, Key Eng. Mater. **103** (1995) 51.

[11] B.S. Bokstein and Z.S. Zsukhovicki, Thermodynamics and kinetics of diffusion in solids (in Russian), Moscow: Metallurgya, 1974, p. 169.

[12] R.S. Barnes and D.J. Mazey, Acta Metall. **6** (1958) 1.

[13] Yu.E. Geguzin, Dokl. Akad. Nauk. SSSR (in Russian) **5** (1956) 839.

[14] Z. Erdélyi and D.L. Beke, J. Mater. Sci. **46** (2011) 6465.

[15] D.L. Beke and Z. Erdélyi, Phys. Rev. B **73** (2006) 035426-1-7.

[16] L.G. Harrison, Trans. Faraday Soc. **57** (1961) 1191.

[21] I. Kaur, Y. Mishin and W. Gust, Fundamentals of Grain and Interphase Boundary Diffusion. Chichester: John Wiley, 1995.

[18] A.D. LeClaire, Br. J. Appl. Phys. **14** (1963) 351.

[19] D.L. Beke, G.A. Langer, G. Molnár, G. Erdélyi, G.L. Katona, A. Lakatos and K. Vad, Phil. Mag. **93** (2013) 1960.

[20] G. Erdélyi, W. Lojkowski, D.L. Beke, I. Gödény and F.J. Kedves, Phil. Mag. **56** (1987) 673.

[21] B. Bokstein, V. Ivanov, O. Oreshina, A. Peteline and S. Peteline, Mater. Sci. Eng. A **302** (2001) 151.

[22] G. Schmitz, D. Baither, M. Kasparzak, T.H. Kim and B. Krause, Scripta Mater. **63** (2010) 484.

[23] V.M. Koshevich, A.N. Gladkikh, M.V. Karpovskyi and V.N. Klimenko, Interface Sci. **2** (1994) 261.

[24] L.N. Paritskaya, Yu. Kaganovskii and V.V. Bogdanov, Solid State Phenom. **101–102** (2005) 123.

[25] M. Kajihara and W. Gust, *Acta metall, mater.* **39** (1991) 2565.

[26] C.R.M. Grovenor, Acta Metall. **33** (1985) 579.

[27] M. Kajihara, Scripta Mater. **54** (2006) 1767.

[28] O. Penrose, Acta Mater. **52** (2004) 3901.

[29] D.N. Yoon, Rev. Mater. Sci. **19** (1989) 43.

[30] S. Inomata and M.O.M. Kajihara, J. Mater. Sci. **46** (2011) 2410.

[31] F. Hartung and G. Schmitz, Phys. Rev. B **64** (2001) 245418.

[32] D. Baiter, T.H. Kim and G. Schmitz, Scripta Mater. **58** (2008) 99.

[33] J. Sheng, U. Welzel and E.J. Mittemeijer, Z. Kristallogr. Suppl. **30** (2009) 247.

[34] M. Hillert and G.R. Purdy, Acta Metall. **26** (1978) 333.

[35] D.L. Beke, Z. Erdélyi and G.L. Katona, Diffusion Foundations **2** (2014) 107.

[36] D.L. Beke, Interdiffusion along grain boundaries – Cold homogenization of thin films, unpublished.

[37] P. G. Shewmon, Acta Metall. **22** (1981) 1567.

[39] L. Klinger and E. Rabkin, Acta Mater. **55** (2007) 4689.

[40] R.W. Balluffi and J.W. Cahn, Acta Metall. **29** (1981) 493.

[41] T. Takenaka and M. Kajihara, Mater. Trans. **47** (2006) 822.

[42] J. Chakraborty, U. Welzel and E.J. Mittemeijer, J. of Appl. Phys. **103** (2008) 113512.

[43] A. O'Neill, R. Agaiby, S. Olsen, Y. Yang, P.-E. Hellstrom, M. Ostling, M. Oehme, K. Lyutovich, E. Kasper, G. Eneman, P. Verheyen, R. Loo, C. Claeys, C. Fiegna and E. Sangiorgi, Appl. Surf. Sci. **254** (2008) 6182.

[44] W. Huang, L. Zhang, Y. Gao and H. Jin, Microelectronic Engineering **84** (2007) 678.

[45] Xin-Ping Qu, Yu-Long Jiang, Guo-Ping Ru, Fang Lu, Bing-Zong Li, C. Detavernier and R.L. Van Meirhaeghe, Thin Solid Films **462–463** (2004) 146.

[46] M. Gregoire, R. Beneyton, S. Del Medico and S. Zoll, Microelectronic Engineering **88** (2011) 548.

[47] Jun Luo, Zhi-Jun Qiu, Jian Deng, Chao Zhao, Junfeng Li, Wenwu Wang, Dapeng Chen, Dongping Wu, Mikael Östling, Tianchun Ye and Shi-Li Zhang, Microelectronic Engineering **120** (2014) 178.

[48] Jian Deng, Qingbo Liu, Chao Zhao, Junfeng Li, Wenwu Wang, Dapeng Chen, Tianchun Ye and Jun Luo, Vacuum **99** (2014) 225.

[49] F. Panciera, K. Hoummada, C. Perrin, M. El Kousseifi, R. Pantel, M. Descoins, M. Gregoire, M. Juhel and D. Mangelinck, Microelectronic Engineering **120** (2014) 34.

[50] J. Luo, Z. Qiu, C. Zha, Z. Zhang, D. Wu, J. Lu, J. Åkerman, M. Östling, L. Hultman and S.-L. Zhang, Appl. Phys. Lett. **96** (2010) 031911.

[51] Z. Zhang, S.-L. Zhang, B. Yang, Y. Zhu, S.M. Rossnagel, S. Gaudet, A.J. Kellock, J. Jordan-Sweet and C. Lavoie, Appl. Phys. Lett. **96** (2010) 071915.

[52] K. De Keyser, C. Van Bockstael, R.L. Van Meirhaeghe, C. Detavernier, E. Verleysen, H. Bender, J. Jordan-Sweet and C. Lavoie, Appl. Phys. Lett. **96** (2010) 173503.

[53] Z. Zhang, B. Yang, Y. Zhu, S. Gaudet, S. Rossnagel, A.J. Kellock, A. Ozcan, C. Murray, P. Desjardins, S.-L. Zhang, J. Jordan-Sweet and C. Lavoie, Appl. Phys. Lett. **97** (2010) 252108.

[54] T.B. Massalski, Binary alloy phase diagrams, second edition, ASM, 1992, volume 3, p. 2860.

[55] M. Putero, L. Ehouarne, E. Ziegler and D. Mangelinck, Scripta Materialia **63** (2010) 24.

[56] W.K. Chu, S.S. Lau, J.W. Mayer, H. Müller and K.N. Tu, Thin Solid Films **25** (1975) 393.

[57] F. Panciera, K. Hoummada, M. Gregoire, M. Juhel, N. Bicais and D. Mangelinck, Appl. Phys. Lett. **99** (2011) 051911.

[58] J. Fouet, M. Texier, M.-I. Richard, A. Portavoce, D. Mangelinck, C. Guichet, N. Boudet and O. Thomas, Materials Letters **116** (2014) 139.

[59] A. Lakatos, G. A. Langer, A. Csik, C. Cserhati, M. Kis-Varga, L. Daroczi, G. L. Katona, Z. Erdélyi, G. Erdelyi, K. Vad and D. L. Beke, Appl. Phys. Lett. **97** (2010) 233103.

[60] L.A. Clevenger and C.V. Thompson, J. App. Phys. **67** (1990) 1325.

[61] M. Ibrahim, B. Parditka, A. Fuhrich. Z. Balogh, P. Stender, Z. Erdelyi and G. Schmitz, Phys. Stat. Sol. C **10** (2013) 1724.

[62] W.H. Wang, H.Y. Bai and W.K Wang, Mat. Sci. and Eng. A **179/A180** (1994) 229.

[63] J.O. Olowolafe, M.A. Nicolet and J. W. Mayer, Thin Solid Films **38** (1976) 143.

[64] J.C. Ciccariello, S. Poize and P. Gas, J. of Appl. Phys. **67** (1990) 335.

[65] F. Nemouchi , D. Mangelinck, C. Bergman, P. Gas and U. Smtith, Appl. Phys. Lett. **86** (2005) 041903.

[66] C. Lavoie, C. Detavernier, C. Cabral Jr., F.M. d'Heurle, A.J. Kellock, J. Jordan-Sweet and J.M.E. Harper, Microelectronic Engineering **83** (2006) 2042.

[67] K.N. Tu, W.K. Chu and J.W. Mayer, Thin Solid Films **25** (1975) 403.

[68] K. Hummada, E. Cadel. D. Mangelinck, C. Perrin-Pelegrino, D. Blavette and B. Deconihout, Appl. Phys. Lett. **89** (2006) 181905.

[69] K. Hummada, C. Perrin-Pellegrino and D. Mangelinck, J. of Appl. Phys. **106** (2009) 063511.

[70] D. Mangelinck, K. Hoummada, A. Portavoce, C. Perrin, R. Daineche, M. Descoins, D.J. Larson and P.H. Clifton, Scripta Mat. **62** (2010) 568.

[71] D. Mangelinck and K. Hummada, Appl. Phys. Lett. **92** (2008) 254101.

[72] J. Demeulemeester, D. Smeets, C. Van Bockstael, C. Detavernier, C.M. Comrie, N.P. Barradas, A. Vieira and A. Vantomma, Appl. Phys. Lett. **93** (2008) 261912.

[73] F.J. Broeder, Thin Solid Films **124** (1985) 135-148

[74] G. Martin, D. Blackburn and Y. Adda, Phys. Stat. Sol. **23** (1967) 223.

[75] N.L. Peterson, in "Diffusion in Metals and Alloys" (eds. F. J. Kedves and D. L. Beke) Diffusion and Defect Monograph Series 7, Trans. Tech. 1983 pp. 145-162

[76] F.J. Broeder and S. Nakahara, Scripta Met. **17** (1983) 399.

[77] E. Rabkin, L Klinger, T. Izyumova and V.N. Semenov, Scripta Mat. **42** (2000) 1031.

[78] L. Daróczi, D.L. Beke, G. Langer, Gy. Radnóczi and Zs. Czigány, J of Magn. and Magn. Mat. **156** (1996) 417.

[79] H. Oechsner, in The Physics of Ionized Gases, (edited by M.M. Popovic) Published by World Scientific, 1985, p.571.

[80] H. Mönig, C. A. Kaufmann, Ch.-H.Fischer, A. Grimm, R. Caballero, B. Johnson, A. Eicke, M. Ch. Lux-Steiner and I. Lauermann, J. Appl. Phys. **110** (2011) 093509.

[81] H. Oechsner, R. Getto and M. Kopnarski, J. Appl. Phys. **105** (2009) 063523.

[82] K.H. Müller and H. Oechsner, Mikrochim. Acta **10** (1983) 51.

[83] A. Wucher, H. Oeschner and Z. Fresenius, Anal. Chem. **333** (1989) 470.

[84] D.B. Williams and C.B. Carter, Transmission Electron Microscopy, Plenum Press, New York, 1996, Vol. 1–4.

[85] B.D. Cullity, Elements of X-ray Diffraction, Addison-Wesley, Reading, MA, 1979.

[86] J.C. Ciccairello, S. Poise and P. Gas, J. of Appl. Phys. **67** (1990) 3315.

[87] Ya.Ye. Geguzin, Yu.S. Kaganovskii and L.N. Paritskaya, Phys. Met. Metall. **54** (1982) 120.

[88] V.M. Kosevich, A.N. Gladkikh, M.V. Karpovskyi and V.N. Klimenko, Interface Science **2** (1994) 261.

[89] G.L. Katona, I.A. Vladymyrskyi, I.M. Makogon, S.I. Sidorenko, F. Kristály, L. Daróczi, A. Csik, A. Liebig, G. Beddies, M. Albrecht and D.L. Beke, Appl. Phys. A. **115** (2014) 203.

[90] G. Molnar, G. Erdelyi, G. Langer, D.L. Beke, A. Csik, M. Kis-Varga and A. Dudas, Vacuum **98** (2013) 70.

[91] O.P. Pavlova, T.I. Verbitska, I.A. Vladymyrskyi, S.I. Sidorenko, G.L. Katona, D.L. Beke, G. Beddies, M. Albrecht and I.M. Makogon, Appl. Surf. Sci. **266** (2013) 100.

[92] C.Y. Ma, E. Rabkin, W. Gust and S.E. Hsu, Acta metall. mater. **43** (1995) 3113.

[93] Y. Yamamoto, S. Uemura, K. Yoshida and M. Kajihara, Mat. Sci. Eng. A **303** (2002) 262.

[94] L. Chongmo and M. Hillert, Acta Metall. **29** (1981) 1949.

[95] J.D. Pan and R.W. Balluffi, Acta Metall. **30** (1982) 861.

[96] F.M. d'Heurle, J. Mater. Res. **3** (1988) 167.

[97] F.M. d'Heurle and P. Gas, J. Mater, Res. **1** (1986) 205.

[98] P. Gas and F.M. d'Heurle, Appl. Surf. Sci. **73** (1993) 153.

[65] F. Nemouchi, D. Mangelinck, C. Bergman and P. Gas, Appl. Phys Lett. **86** (2005) 041903.

[99] K. Hoummada, D. Mangelinck and A. Portavoce, Solid State Phenom. **172-174** (2011) 640.

[100] H. Fricke, Phys. Rev. **24** (1924) 575.

[101] U. Gossele and K.N. Tu, J. Appl. Phys. **53** (1982) 3252.

[102] A. Lakatos, G. Erdelyi, G.A. Langer, L. Daroczi, K. Vad, A. Csik, A. Dudas and D.L. Beke, Vacuum **84** (2010) 953.

[103] S. Coffa, J.M. Poate, D.C. Jacobs, W. Frank and W. Gustin, Phys. Rev. B **43** (1992) 8355.

[104] J.D. Pan and R.W. Balluffi, Acta Metall. **30** (1982) 861.

[105] J. Sommer, Y.M. Chiang and R.W. Balluffi, Scripta Met. et Mat. **33** (1995) 7.

[106] F.J.A. Den Broeder, Acta Metall. **20** (1972) 319.

Publications

1. Scientific papers related to the dissertation

1- "Production of NiSi phase by grain boundary diffusion induced solid state reaction between Ni_2Si and Si(100) substrate"
S.S. Shenouda, G.A. Langer, G.L. Katona, L. Daróczi, A. Csik, and D.L. Beke,
Applied Surface Science, **320** (2014) 627, cited by (1).
Impact Factor: 2.711

2- "Kinetics of shift of individual interfaces in Ni/Si system during low temperature reactions"
S.S. Shenouda, G. Molnar, G.A. Langer, G.L. Katona, F. Kristaly and D.L. Beke,
Microelectronic Engineering, **134** (2015) 14.
Impact Factor: 1.197

3- "Nanoscale Kirkendall porosity formation during grain boundary intermixing in Au/Ag thin film system"
S.S. Shenouda, G.L. Katona, G.A. Langer, L. Daróczi and D.L. Beke,
Materials Letters, **145** (2015) 67.
Impact Factor: 2.489

4- "Eljárás kontrollált vastagságú nanoréteg előállítására és ilyen eljárással előállított nanoréteg" c.
Hungarian patent registration No. P1400230/2014,
S.S. Shenouda, G.A. Langer, G.L. Katona, S. Kéki, M. Zsuga, and D.L. Beke.

5- "Investigation of solid state reactions between Ni_2Si nanocrystalline film and Si Substrate"
S.S. Shenouda, G.A. Langer, A. Csik, G.L. Katona and D.L. Beke**,**
Acta Physica Debrecina, **47** (2013) 175.

2. Other scientific papers

6- "Electrical properties of $ZnGa_2Se_4$ defect chalcopyrite thin films"
M. Fadel, I.S. Yahia, G.B. Sakr and **S.S. Shenouda**,
Proceedings of "The 2nd International Conference on Advanced Materials and their Applications" and its workshop on "New Trends on Nanoscience and Laser Physics", 2010, NRC, Cairo, p.107.

7- "Memory switching of $ZnGa_2Se_4$ thin films as a new material for phase change memories (PCMs)"
I.S. Yahia, M. Fadel, G.B. Sakr and **S.S. Shenouda**,
Journal of Alloys and Compounds **507** (2010) 551, cited by (15).
Impact Factor: 2.134

8- "Analysis of current–voltage characteristics of Al/p-$ZnGa_2Se_4$/n-Si nanocrystalline heterojunction diode"
I.S. Yahia, M. Fadel, G.B. Sakr, F. Yakuphanoglu, **S.S. Shenouda** and W.A. Farooq,
Journal of Alloys and Compounds **509** (2011) 4414, cited by (20).
Impact Factor: 2.289

9- "Impedance spectroscopy of nanostructure p-$ZnGa_2Se_4$/n-Si heterojunction diode"
I.S. Yahia, M. Fadel, G.B. Sakr, **S.S. Shenouda**, F. Yakuphanoglu, and W.A. Farooq,
Acta Physica Polonica A **120** (2011) 563, cited by (6).
Impact Factor: 0.444

10- "Effect of the frequency and temperature on the complex impedance spectroscopy (*C-V* and *G-V*) of p-$ZnGa_2Se_4$/n-Si nanostructure heterojunction diode"
I.S. Yahia, M. Fadel, G.B. Sakr, **S.S. Shenouda**, and F. Yakuphanoglu,

Journal of Materials Science **47** (2012) 1719, cited by (6).
Impact Factor: 2.163

11- "Structure, optical spectroscopy and dispersion parameters of $ZnGa_2Se_4$ thin films at different annealing temperatures"
M. Fadel, I.S. Yahia, G.B. Sakr, F. Yakuphanoglu and **S.S. Shenouda**,
Optics Communications **285** (2012) 3154, cited by (2).
Impact Factor: 1.438

12- "Negative capacitance of $ZnGa_2Se_4$/Si nano-heterojunction diode"
I.S. Yahia, G.B. Sakr, **S.S. Shenouda**, M. Fadel, S.S. Fouad and F. Yakuphanoglu,
Applied Physics A: materials science and Processing, **112** (2013) 275, cited by (4).
Impact Factor: 1.694

13- "Investigation of solid state reaction in Ag/Sn nanostructured thin films at room temperature"
N. Samy, **S.S. Shenouda**, M. Fadel, H.Talaat, G.L. Katona, G.A. Langer, A. Csik and D.L. Beke,
Submitted to Philosophical Magazine.

3. Conferences (presentations and posters) related to the dissertation

1- Presentation in "The 3rd Scientific Workshop for Egyptian researchers" May 2, 2013 Vienna, Austria.
With title: "Solid state reactions between Ni_2Si nanocrystalline film and Si substrate"

2- Poster in "The 9th International Conference on Diffusion in Solids and Liquids" (DSL-2013) June 24-28, Madrid, Spain.
With title: "Solid state reactions between Ni_2Si nanocrystalline film and Si substrate"

3- Presentation in "The 4th Scientific Workshop for Egyptian researchers" June 22, 2014 Vienna, Austria.
With title: "Nanoscale investigations of solid state reactions and shift of individual interfaces in Ni/c-Si system by Secondary Neutral Mass Spectrometry".

4- Presentation in "The International Conference & Exhibition on Advanced & Nano Materials" (ICANM-2014) August 11-13, Calgary, Alberta, Canada.
With title: "Nanoscale investigations of solid state reactions and shift of individual interfaces in Ni/crystalline-Si system by secondary neutral mass spectrometry".

5- Poster in "The International Conference on Diffusion in Materials" (DIMAT 2014) August 17-22, Münster, Germany.
With title: "Nanoscale investigations of solid state reactions and shift of individual interfaces in Ni/amorphous-Si system by Secondary Neutral Mass Spectrometry".

6- Poster in "International Conference on Smart Materials for shaping our future" (SMART 2014) September 20-21, Debrecen, Hungary.
With title: "Nanoscale investigations of diffusion and solid state reactions in Ni/Si systems".

7- Poster in "The 11th International Conference on Diffusion in Solids and Liquids" (DSL-2015) June 22-26, Munich, Germany.
With title: "Grain boundary intermixing in Ag/Au thin film system and nanoscale Kirkendall porosity formation".

4. Other conferences

8- Presentation in "The 2nd International Conference on Advanced Materials and their Applications and its workshop on New Trends on Nanoscience and Laser Physics", April 6-8, 2010, NRC, Cairo, Egypt.
With title: "Electrical properties of $ZnGa_2Se_4$ defect chalcopyrite thin films"

Acknowledgment

First and foremost, all praise and thanks goes to God who helped me to carry out this work and for the many blessings bestowed upon me.

I would like to express my sincere thanks to my supervisor, Prof. Dr. Dezső L. Beke, for accepting me into his scientific research group. It has been an honor to be his PhD student. This thesis would never have happened without his constant guidance, encouragement, knowledge and ideas which have been a great resource and inspiration. He has always been available to provide assistance and to explain the underlying science and how good experimental physics could be done. His enthusiasm and joy are contagious and motivational for me. I am thankful for the excellent example he has provided as a kind father, ideal character, expert physicist and successful professor.

I would like to express my gratitude to the Department of Solid State Physics – Faculty of Science and Technology – University of Debrecen and the Institute of Nuclear Research (ATOMKI) in Debrecen, Hungary. My sincere thanks go to Dr. Zoltán Erdélyi the head of the Department of Solid State Physics and to Dr. István Szabó the former head of the department.

I'm extremely grateful to Dr. Gábor Langer for his advices and for the countless discussion we had related to the experimental work. Also, I am would like to express my great thankful to Dr. Gábor

Katona for helping me and teaching me a lot of things. I am extremely thankful also to Dr. Lajos Daróczi and Dr. Attila Csik who helped me in doing some of the experiments. Also, I would like to thank all the co-workers for their contributions.

My sincere thanks go to Dr. Gábor Erdélyi, Dr. Csaba Cserháti. Also, I am thankful to Prof. Dr. Kálmán Vad.

I would like to thank my colleagues: Dr. Tarek El Rasasi, Dr. Yusuke Iguchi, Dr. Bence Parditka, Dr. Viktor Takáts, Dr. Istvan Csarnovics, Soha Ferenc, Szilvia Gyöngyösi, Gábor Molnár, János Tomán, László Zoltán Tóth, … to all the others.

I would like to thank the administrative stuff of the department (Éva Kosztyuné Gottfried, Katalin Bakóné Kósa and Julika Gargya Józsefné) and the secretary of the PhD School, Dr. Dorottya Sohler. Also, I would like to thank Dr. Zsuzsanna Bokor.

I would like to express my gratitude to the Hungarian Scholarship Board (HSB), the Ministry of Higher Education in Egypt and the Egyptian Culture Office in Vienna.

I would like also to express my gratitude to the OTKA Board of Hungary (No. CK80126), and to the TAMOP 4.2.2.A-11/1/KONV-2012-0036 and TAMOP-4.2.2/B-10/1-2010-0024 projects (implemented through the New Hungary Development Plan co-financed by the European Social Fund and the Euro*pean Regional Development Fund).*

Last but not the least, I would like to express my great thankful to my family especially to my parents, my brother Mina, my future wife, Dr. Milad Sobhy and his wife for their continuous support, without them I couldn’t make it through.